Marine Structures 100 (2025) 103732

Contents lists available at ScienceDirect

Marine Structures

journal homepage: www.elsevier.com/locate/marstruc

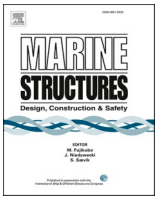

Ultra-low cycle fatigue of ship hull structure – an alternately-cyclically loaded four-point bending test of a large box girder

Shi Song [a,*], Sören Ehlers [b], Franz von Bock und Polach [a], Moritz Braun [b]

[a] Hamburg University of Technology (TUHH), Institute for Ship Structural Design and Analysis (M-10), Am Schwarzenberg Campus 4 C 21073 Hamburg, Germany

[b] German Aerospace Center (DLR), Institute of Maritime Energy Systems, Düneberger Str. 108 21502 Geesthacht, Germany

ARTICLE INFO

Keywords:
Large complex structure
Ship structure
Steel structure
4-point bending
Ultra-low cycle fatigue
Large scale test

ABSTRACT

Ultra-low cycle fatigue (ULCF) refers to material failure at small number of loading cycles. For large complex structures like ships, the damage from ULCF can bring hazardous consequences. In this study, an alternately-cyclically loaded four-point bending test of a large box girder is introduced as the specimen to represent the ULCF of ship hull structure. In every load during the test, large deformation is applied to the specimen even after reaching its ultimate hull girder strength (UHGS), thus extensive plastic deformation and obvious fracture can occur in the specimen. The severely damaged specimen is further tested until 1.5 cycles of bending are finished, thus the test of post-damage box girder is realized. Moreover, the box girder is divided into 3 sub-sections, which show different but still interacting structural behavior. The result of the test shows the structural behavior of a large complex structure suffering severe damage during alternate hogging and sagging after reaching its UHGS, which corresponds to the consequence of ULCF. The presented ULCF test also provides experiences for investigations of large complex structures with existing damages or after accidental loads. Considering the number of cycles in the test, this study can bridge the gap between monotonic overload and ultra-low cycle fatigue.

Introduction

For steel structures under cyclic loading, ultra-low cycle fatigue (ULCF) refers to material failure at very small number of cycles (e.g., <100 cycles [1] or <10–20 cycles [2–6]), and often includes large plastic strains [1,5,6]. Considering large complex structures like ships under cyclic loading, during the loading process, if the load continues after reaching the ultimate hull girder strength (UHGS) (which is called as 'further load after UHGS' in this study), the structure is prone to ULCF. The resultant consequence can be hazardous, an example is the total collapse of the MOL Comfort [7], which is possibly caused by further load after UHGS [8].

Many researches, including tests, have been carried out about the structural strength of ship hull structures [9]. For example, Sugimura et al. made a destructive experiment of a 1/5 scale ship hull model [10]. Paik et al. tested the ultimate strength reduction characteristics of a cracked steel plate subjected to axial tension/compression [11]. Ringsberg et al. carried out a test of a stiffened

* Corresponding author.
E-mail addresses: shi.song@tuhh.de (S. Song), soeren.ehlers@dlr.de (S. Ehlers), franz.vonbock@tuhh.de (F. von Bock und Polach), moritz.braun@dlr.de (M. Braun).

https://doi.org/10.1016/j.marstruc.2024.103732
Received 12 September 2024; Received in revised form 7 November 2024; Accepted 20 November 2024
Available online 29 November 2024

plate structure subjected to uniaxial compressive loads [12]. Wang et al. investigated the ultimate longitudinal strength of a scaled ultra large container ship structure via bending test [13]. However, to reveal structural behavior during ULCF, cyclic loading is needed instead of monotonic overload. During cyclic loading, the accumulated damage brings imperfections to the following cycles. The imperfections will influence the structural strength and other structural behaviors [14].

For cyclic loading and collapse of ship hull-like structures, many analytical works have been done [15–19]. Studies of low-cycle fatigue (LCF) are often based on assumptions limiting the extent of damage [19]. In contrast, in ULCF, the extent of damage is supposed to be high. Due to the difference between LCF and ULCF [20], efficient criterion of ULCF should be considered and incorporated into existing cyclic progressive collapse method [15]. This brings the requirement of investigations about the ULCF of ship hull structures, including experiments like large-scale test with cyclic loading.

The cyclic loading is often categorized into two types: pulsating loading and alternate loading. In pulsating loading, loads applied on the specimen are only in one direction, while in alternate loading, loads in opposite directions are applied on the specimen in sequence. Gordo et al. [21–23] and Deng et al. [24] carried out tests on box girder or hull girders subjected to pulsating loading. However, in pulsating loading, either hogging or sagging is considered. This is different from alternate cyclic loading, which includes both hogging and sagging. Hence, alternate cyclic loading can provide more comprehensive results regarding ULCF of ship hull structures. However, only very few amount of large-scale ULCF tests has been carried out with alternate cyclic loading. Fukumoto et al. carried out a series of cyclic bending tests of thin-walled box beams [25], where moderate extent of damage was accumulated, but no severe damage, like large plastic deformation or fracture occurred during the test. Akhras et al. carried out a large-scale bending test of a box girder [26] with three sub-sections in the test area divided by transverse stiffeners. After the first bending, the box was turned and tested again. No fracture was observed in the test. Since the box girder was turned only once, the structural behavior after a full alternate cycle is unknown. Cui et al. carried out a series of cyclic tests of box girders made by 2.76–3.78 mm thick Q235 and Q345 steel [27]. The test area of the box girder is focused on one sub-section stiffened by longitudinal stiffeners. The maximum force and bending moment applied on the specimen was close to 800 kN and 400 kN·m. No fracture was observed from the Q345 specimen.

The research works mentioned above represent ULCF of large steel structure with moderate extent of damage, like plastic deformation and local buckling. However, considering the severity of structural damage in ULCF [7], extensive plastic deformation and even obvious fracture, should be investigated to provide more insight into the consequences of accident, as well as to contribute to development of protections against hazards. Moreover, referring to the collapse of MOL Comfort [7] mentioned above, when damage occurs, it should not only be regarded as the final consequence, but also the initial condition for upcoming loads, since it is possible that an already damaged ship has to continue operating in challenging conditions, or otherwise endure fatal damage. Such extent of damage and load condition during ULCF is not included in any existing research works. This study investigates the ULCF of large steel structure via experiment with severe damage occurred during the test and used as initial condition for following loading. To achieve this, an alternately-cyclically loaded four-point-bending test is introduced, with a large box girder as the specimen for test. In every loading process, the UHGS of the specimen is reached first, then the loading continues, which can cause large plastic strains and even fractures. However, the extent of loading will not introduce total collapse of the specimen in only one loading process. Instead, the occurred damage, including fracture, is used as the imperfection for following loading process within the test. As is mentioned above, once enduring further load after UHGS during cyclic loading, the structure is prone to ULCF. Therefore, the loading configurations in this study can represent ULCF of the specimen.

When investigating ULCF of ship structures via experiment, test setups representing ship structures with higher fidelity is preferable for more comprehensive knowledge. Fidelity of the test setups is represented by e.g., comparable structural dimensions and strength, as well as similar structural layout referring to ship structures. The specimen used in this study is designed to represent simplified ship structures with its dimensions, plate thickness and structural layout. The test area of the specimen is fabricated with 5–8 mm steel plates and is stiffened with 12 longitudinal stiffeners and 4 frames. The maximum force and bending moment applied on the specimen is expected to be higher than 3000 kN and 2000 kN·m respectively. As a result, although not comparable with full-size ship structures, the specimen can provide higher resistance against bending in ULCF, compared with that from existing works. Moreover, similar as that in [26], the test section of the specimen is divided into three sub-sections by transverse frames, which makes the layout of the specimen closer to that of ship structures, which also have multiple sub-sections divided by bulkheads or stiffeners. When a large extent of damage occurs, such layout can reveal structural behaviors from different sub-sections, as well as the interactions between them.

In Section 2, the preparation of the test is described, including design of the specimen, setups of the test, and the measurement of data. In section 3, the results of the test are presented. Based on the sections above, the ultra-low cycle fatigue of the tested large steel structure is discussed in section 4. Following that, the conclusions are summarized in section 5.

Preparation of the test

The preparation of the test is introduced in this section, including the design of the specimen, setup of the test, and measurement of data. More details are further shown in the appendix.

Design of the specimen

In this test, a large box girder with stiffeners is designed to represent a simplified ship hull structure according to the experimental testing capabilities available. The length of the whole specimen is about 6000 mm, while the test part (midsection of the specimen, see Fig. 4) is about 2500 mm in length, 1225 mm in width and 744 mm in height, with hull plate thickness of about 5.66 mm, stiffened with transverse frames (about 8.24 mm thick) and longitudinal stiffeners (about 6.16 mm thick). More details about the design of the box

girder is shown in Fig. 1 and Fig. 35, while the list of the components is shown in Table 1. Outside and inside views of the specimen before test are shown in Figs. 2 and 3.

The specimen is divided into three sections: midsection, aft and forward, see Fig. 4. Referring to the dimensions of components in Table 1, the hull thickness in midsection is smaller than that from aft and forward. Hence, compared with the aft and forward, the midsection is expected to have significant deformation and damages, such as fracture and buckling.

To represent the local positions and deformation after test, grid lines are drawn on the specimen. Moreover, "mesh grids" are also drawn on the top, bottom and starboard of the specimen. The size of the grids is about 25 mm, see Fig. 5.

In the longitudinal direction (along the x-axis), the specimen is divided into 36 divisions. The first and last divisions are at the two ends of the connection plate, see Fig. 4. The IDs for the divisions are numbered as their longitudinal distance from the first division in millimeter, see Fig. 5. Based on the division IDs, the four frames of the specimen are located at division 1125, 1875, 2625 and 3375. These four frames divide the midsections into three sub-sections, namely S1, S2 and S3, see Fig. 4. In this paper, the sub-section always refers to a section of box girder between two adjacent frames.

Test setup

The test is carried out in the laboratory of the Institute for Ship Structural Design and Analysis in Hamburg University of Technology (TUHH). The general layout of the test, including the test rig and the specimen, is shown in Figs. 6 and 7. The horizontal positions of the hydraulic cylinders are also shown in Fig. 37. In this test, four-point bending is achieved via the contact between the specimen and the load introducer, as well as the supports, see Figs. 6 and 7. The load is induced by the hydraulic cylinders. More information regarding the cross beam, the base support structure, and the hydraulic cylinders can be found in [28] and [29]. By operating the hydraulic cylinders, the cross beam carrying the load introducer can move towards the specimen for loading or move away from the specimen for unloading. The load introducer is shown in Fig. 8 and Fig. 36, including two pairs of indenters with spherical head for its contact against the specimen. The support also contacts the specimen via two pairs of support heads. The designs of the support head and indenter are shown Fig. 37. The dimensions of the cross beam are shown in Fig. 38. while "X" shape is designed to transfer the load from hydraulic cylinders to load introducer via the cross beam.

As is mentioned above, the midsection of the specimen has smaller plate thickness and is expected for most deformation and damage. The forward and aft sections have larger plate thickness and higher strength. Hence, to avoid undesired results induced by indirect contact between the midsection and the load introducer or support, the contact points are located at stiffened points on the forward and aft sections, see Fig. 9.

For an ultra-low cycle fatigue test, cyclic loading is essential. In this test, each cycle consists of two half-cycles. In each half-cycle, the specimen is loaded monotonically. Before the next half-cycle, the specimen is turned for 180° about its x-axis, see Fig. 10. After the turning, the specimen is placed back on the test rig and load in the same manner, see Fig. 11. Therefore, it is possible to apply the load in the opposite direction from the last half-cycle. In this test, the specimen is loaded with one and half load cycles (three half-cycles). The load is displacement controlled. In the first half-cycle, the displacement introduced in each hydraulic cylinder is about 70 mm. In the second half-cycle, the displacement introduced in each hydraulic cylinder is about 120 mm, while calibrations are applied considering the different deformation at the forward and aft of the specimen. Combining with the unloaded displacement by elastic deformation (about 20 mm) in the first half-cycle (see Fig. 28), this loading control keeps the same load amplitude in both directions for the first cycle (including the first and second half-cycle), see Figs. 11 and 20. Such extent of load can ensure the occurrence of obvious damage, like plastic deformation and even local fracture, while avoid total collapse of the whole specimen in only one loading

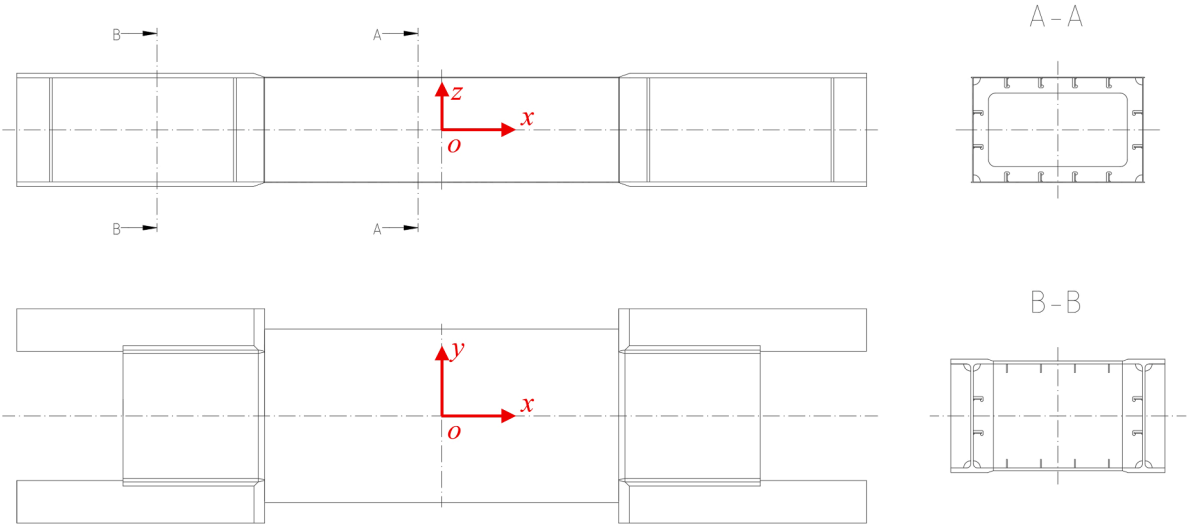

Fig. 1. Three view drawing of the specimen, as well as the definition of its coordinate system. More details are shown in Fig. 35.

Fig. 2. Outside view of the specimen, taken from the stern and starboard side of the specimen.

Fig. 3. Inside view of the specimen.

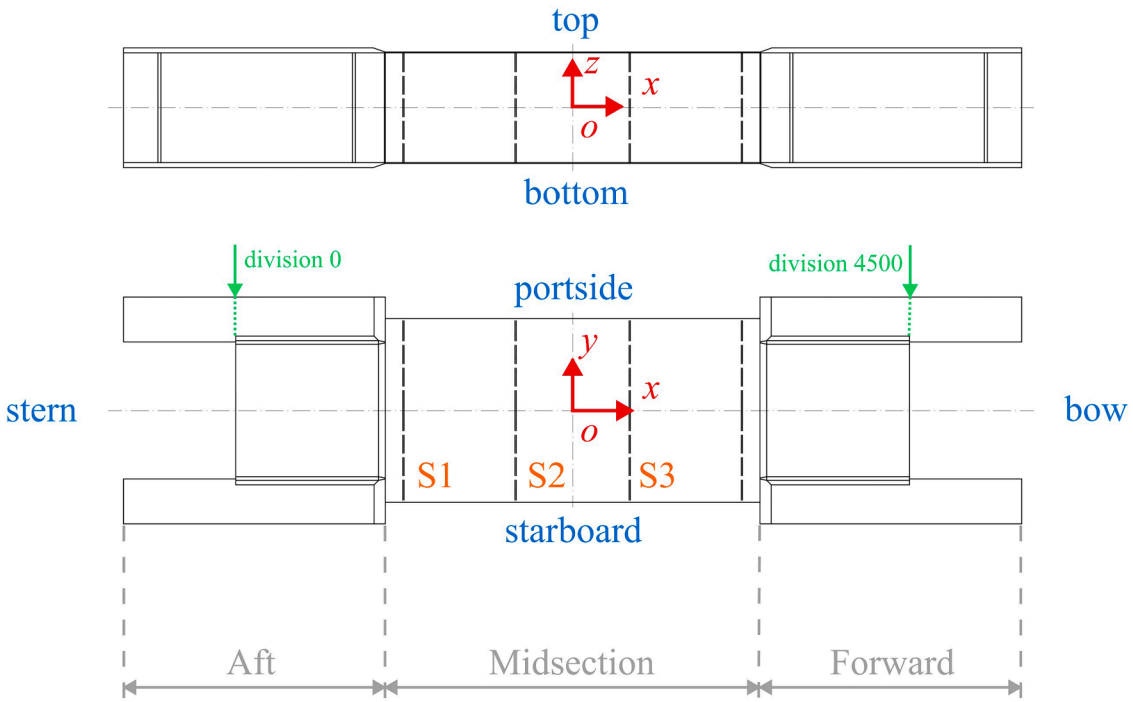

Fig. 4. Definition of directions, sections and divisions of the specimen. S1, S2 and S3 refers to the sub-sections divided by the frames.

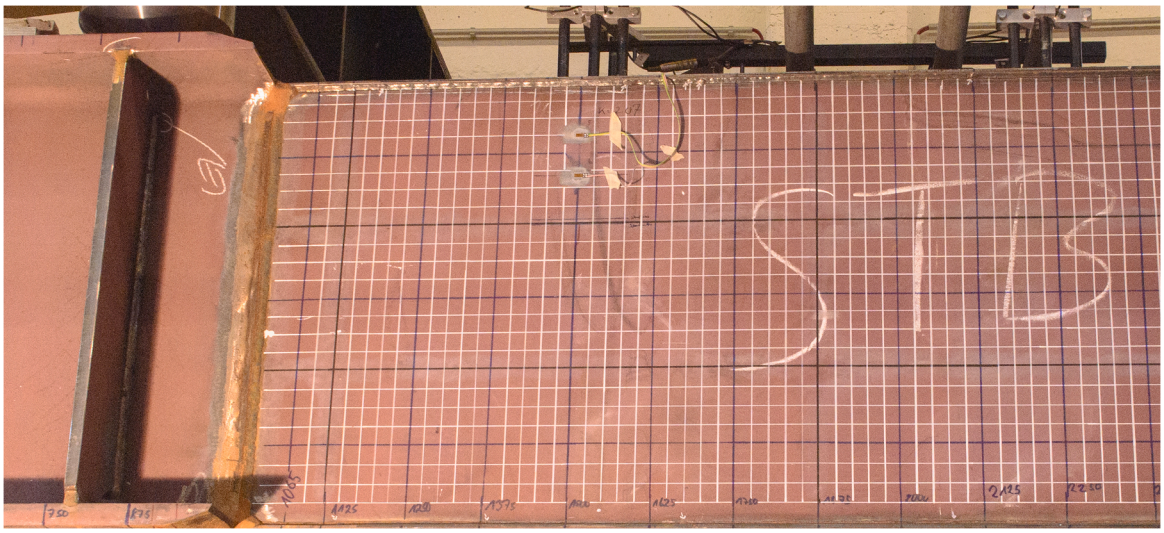

Fig. 5. The divisions and grids drawn on the specimen (starboard). The numbers are the division IDs. The white grid drawn on the specimen has a distance between lines of about 25 mm (except for that between 1065 and 1125).

process. In the third half-cycle, the displacement introduced in each hydraulic cylinder is about 180 mm. During the test, the loading speed in hydraulic cylinder is about 0.1 mm/s, by which the load is regarded as quasi-static. The full load history can be found in section 3.

Due to the imperfections in the specimen and test rig, the specimen can deform unsymmetrically, while the test results cannot be perfectly symmetric as well. To make sure all the indenters have the highest chance to contact the specimen and introduce loads, at the beginning of each half-cycle, all the indenters are moved to the positions where they can contact the specimen at the points showed in Fig. 9. Such calibration of contact is also applied during the first half-cycle and most of the second half-cycle. Relevant results are further shown and discussed in section 3.

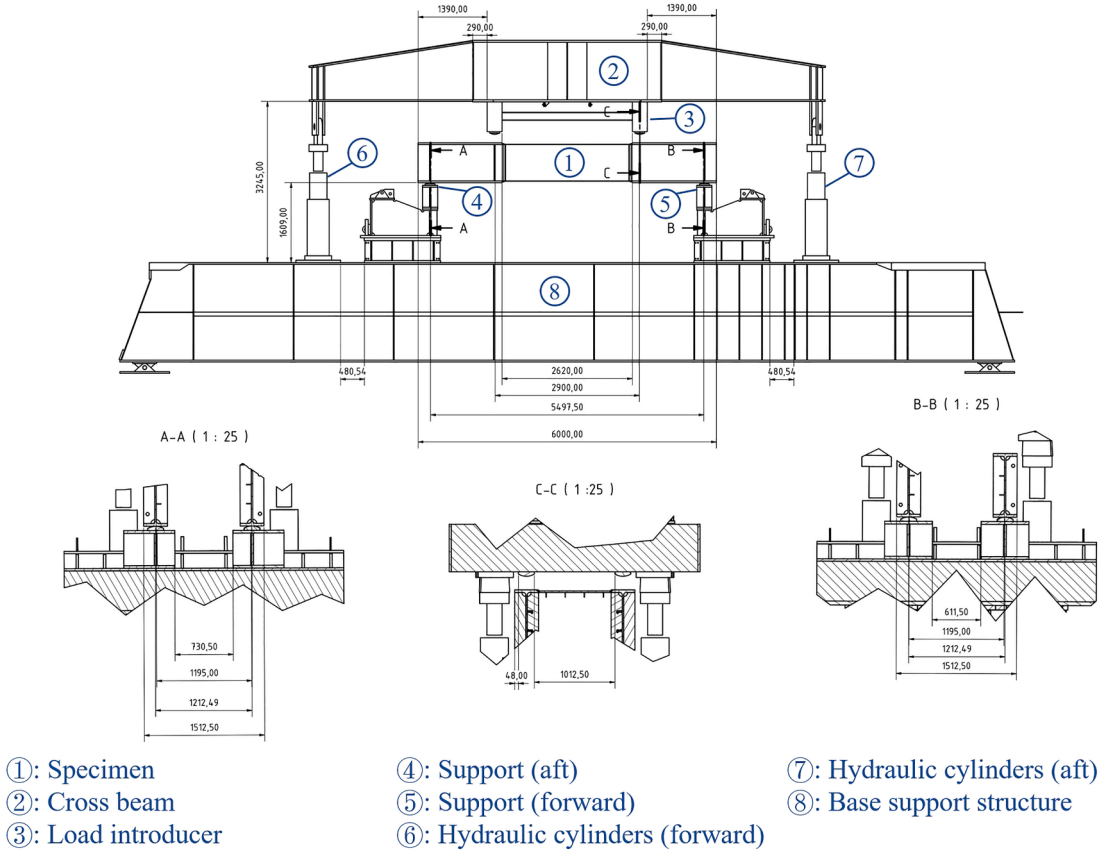

Fig. 6. Layout of the test. The test rig consists of number 2–8 in the picture.

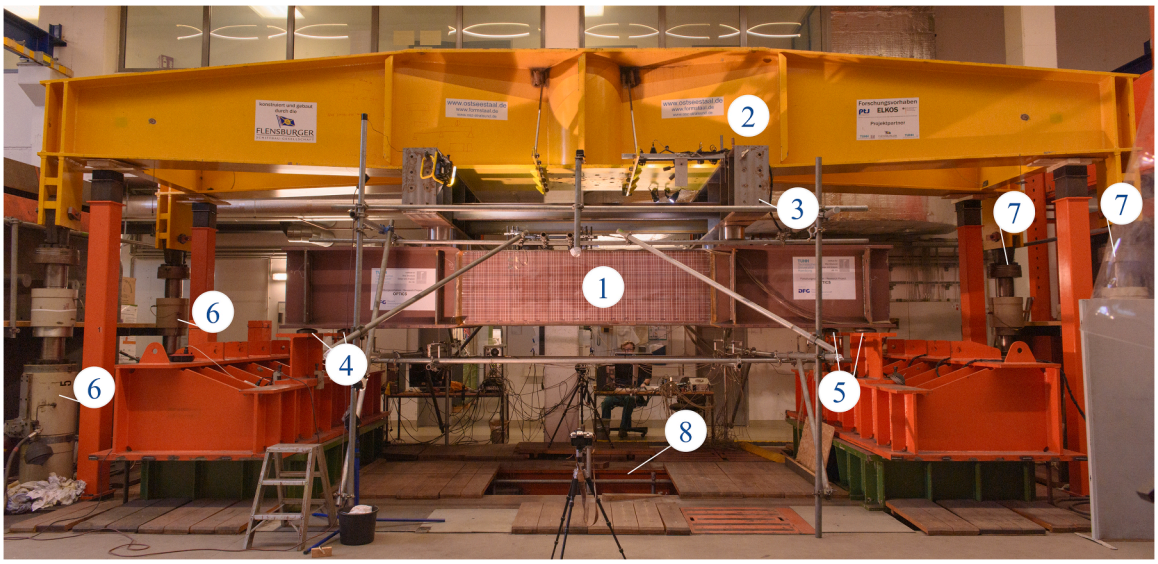

Fig. 7. Photo of the test layout. The numbers here correspond with the numbers in Fig. 6. The base support structure indicated in Fig. 6 is under the ground and not fully visible. This photo is taken from the starboard side of the specimen.

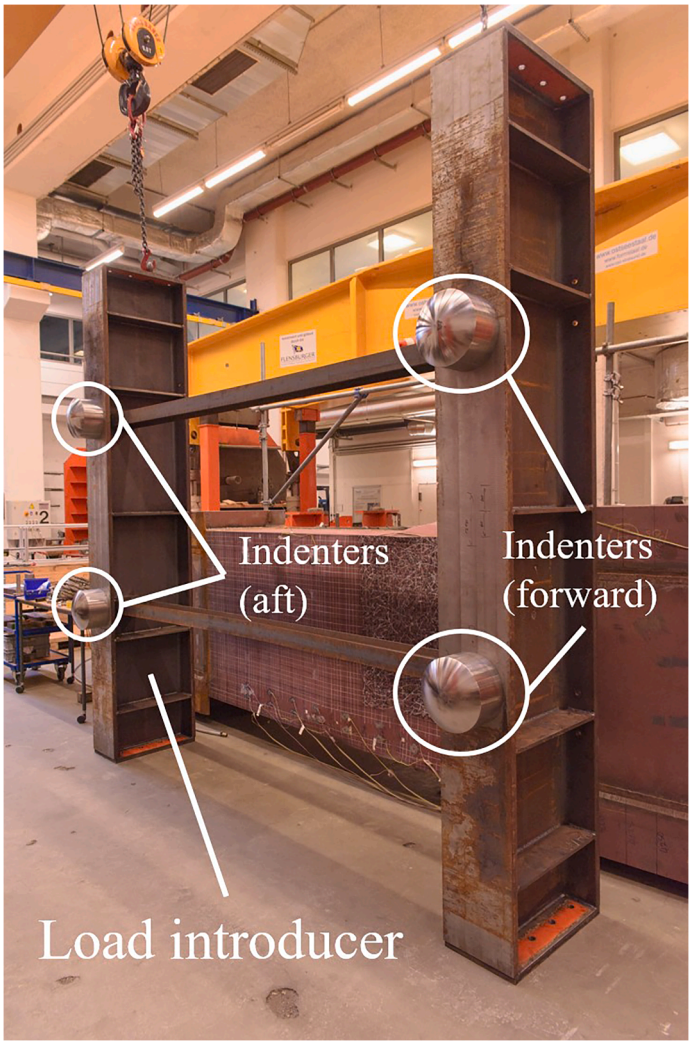

Fig. 8. Photo of the load introducer including the indenters.

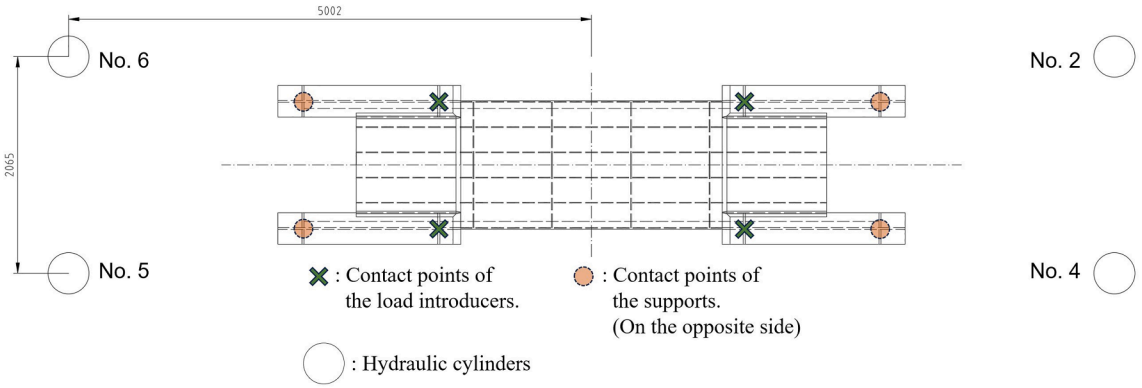

Fig. 9. Positions of the loading, support, and hydraulic cylinders. The view is from the upper side of the specimen.

Fig. 10. Turning of the specimen.

Measurement of data

Before the test and after each half-cycle, the outer hull of the specimen is measured along the divisions by laser scanner or laser rangefinder. Moreover, positions of the stiffeners are measured inside the specimen to indicate the initial imperfections before each half-cycle. The stiffeners are marked in Fig. 12, with the same coordinate system shown in Fig. 4. The initial deflections of the top of the stiffeners are shown in Fig. 13. It can be seen that the initial deflections of the stiffeners are mostly less than their thickness (6.16 mm) within the midsection area. However, large deflection still exists, like the stiffener II between division 3200 and 3300 on portside, see Figs. 13 and 14.

To record the loads, the force and displacement in each hydraulic cylinder are measured respectively. This measurement also includes the unloading at the end of each half-cycle, by which the whole load process are be recorded.

Apart from the quantitative measurements mentioned above, videos were also recorded during the test. Hence, the condition of the specimen, such as deformation, buckling or fracture, can be visualized after the test.

Test results

The results of the test are presented in this section, including the deformation and damage after the first, second or third half-cycle, as well as the resulting data and relevant calibrations. More discussions about the results can be found in the next section.

Deformation and damage

After the first half-cycle, buckling of hull plates, stiffeners and frames were observed, as well as large plastic deformation, see Fig. 15, Fig. 16, and Fig. 17. The largest deformation induced by buckling happens in sub-section S2 and S3. Comparably, the S1 is not very heavily damaged. The extent of damage in these sub-sections are illustrated by the laser scan results of the outer hull surface along division 1375, 2250 and 2875, see Fig. 18. The coordinate system here is based on that shown in Fig. 4.

The overall deformation of the specimen after second half-cycle is shown in Fig. 20. Moreover, apart from buckling, fracture was also observed in the second half-cycle, see Fig. 21, Figs. 22 and 23. Since the loading direction of the second half-cycle is opposite to the first half-cycle, the longitudinal deformation of the box girder is reversed, but the plastic deformation occurred in the first half-cycle

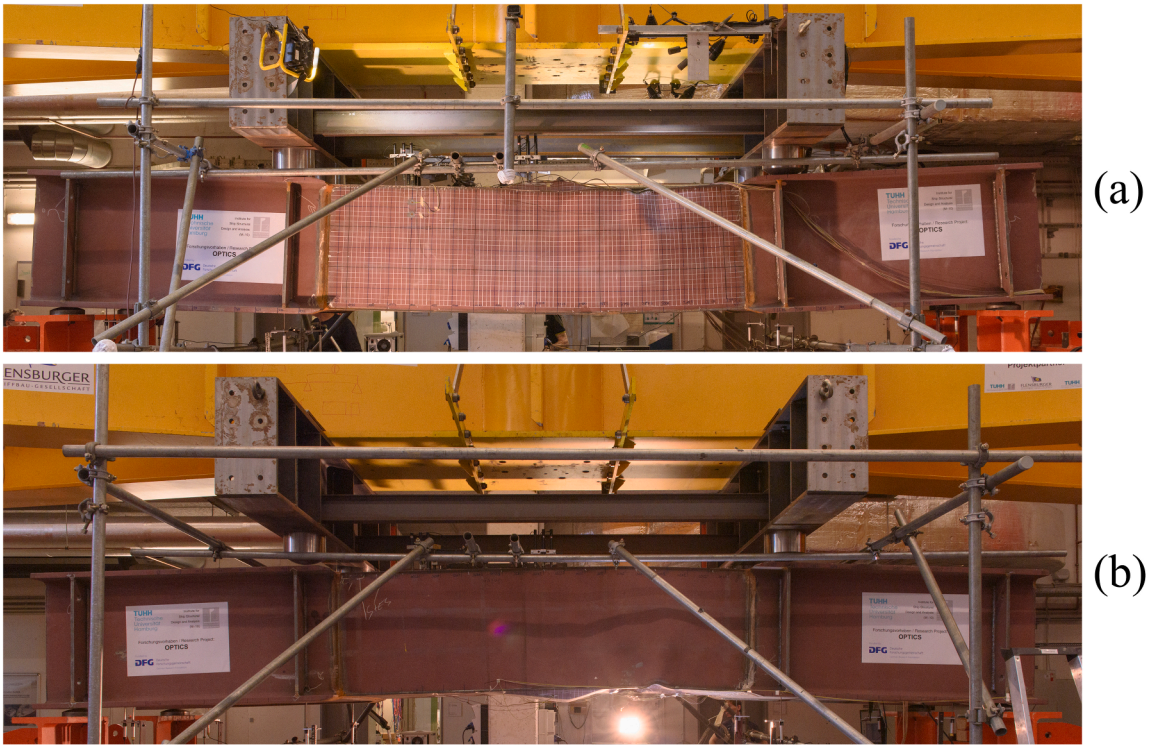

Fig. 11. The specimen after the first half-cycle (a) and before the second half-cycle (b).

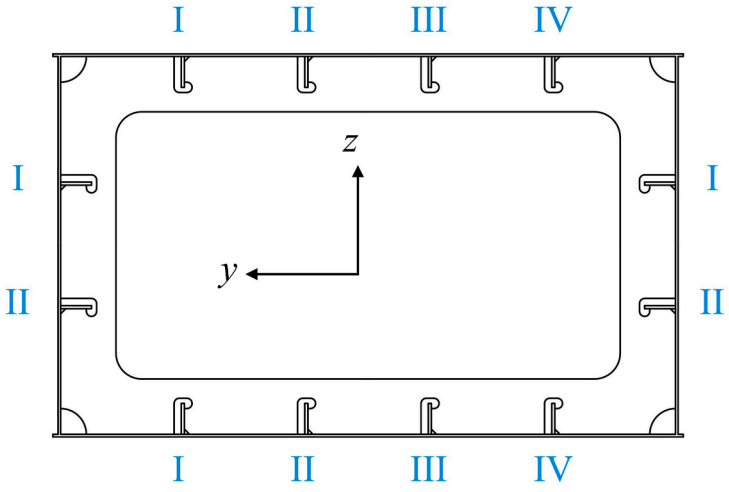

Fig. 12. The marks for the stiffeners.

did not fully "recover" back to what they were before the first half-cycle, see Figs. 17 and 19, whose extent is even higher for the third half-cycle. The remaining damage can cause additional imperfection to the specimen, such as increased initial imperfection of stiffeners, see Fig. 27. This will increase the extent of damage, such as buckling and fracture, in the next half-cycle. Moreover, the endurance of the specimen, such as the UHGS, is also reduced compared to the first half-cycle, see Fig. 34. This will be further presented and discussed in the following sections.

Compared with the second half-cycle, due to higher initial imperfection, including the occurred fracture, the deformation and fracture become more severe after the third half-cycle, see Figs. 18 and 23 to Fig. 26. Considering the Bauschinger effect [30], the existing plastic strain also contributes to easier follow-up plastic deformation and fracture at the position with large deformation [18].

Comparing the deformation of S2 and S3, the extent of damage in S3 is increasingly higher than that in S2. This is same for material fracture, which only occurs in S3. In addition, the frame between S2 and S3 also received heavy damage, which becomes increasingly

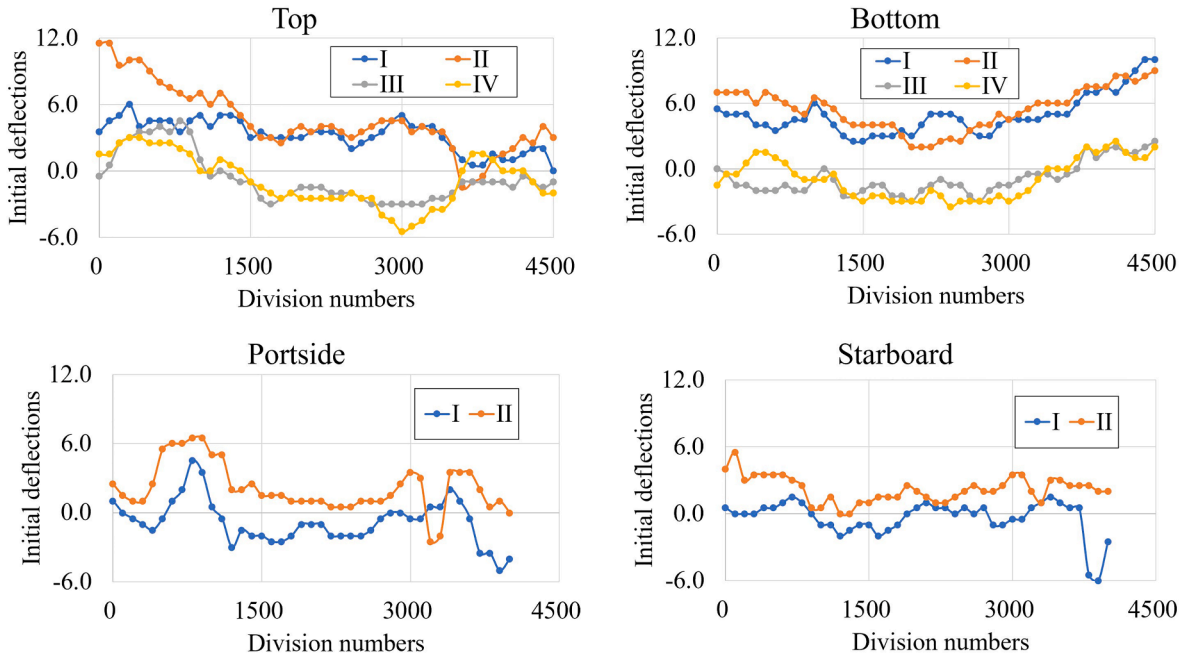

Fig. 13. Initial deflections of the stiffeners.

Fig. 14. Large initial deflections of the stiffener before test.

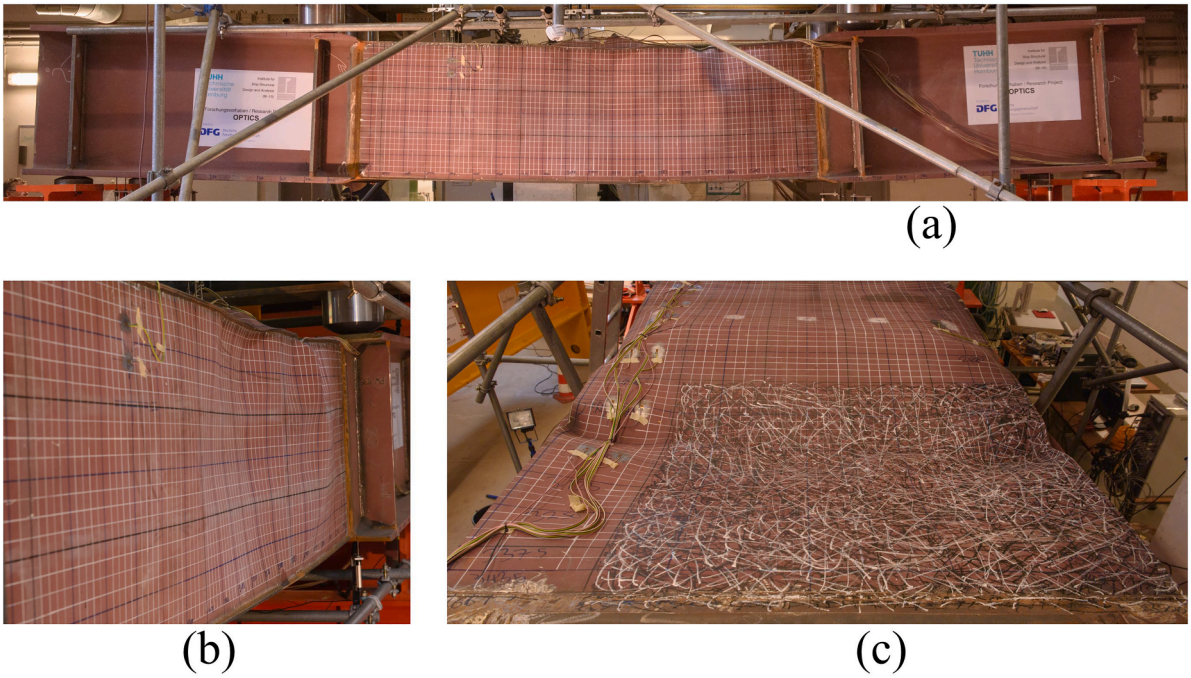

Fig. 15. Deformation of outer hull after 1st half-cycle. (a) shows the overall deformation of the specimen (view from starboard), (b) and (c) shows the local deformation at starboard and top of the specimen respectively.

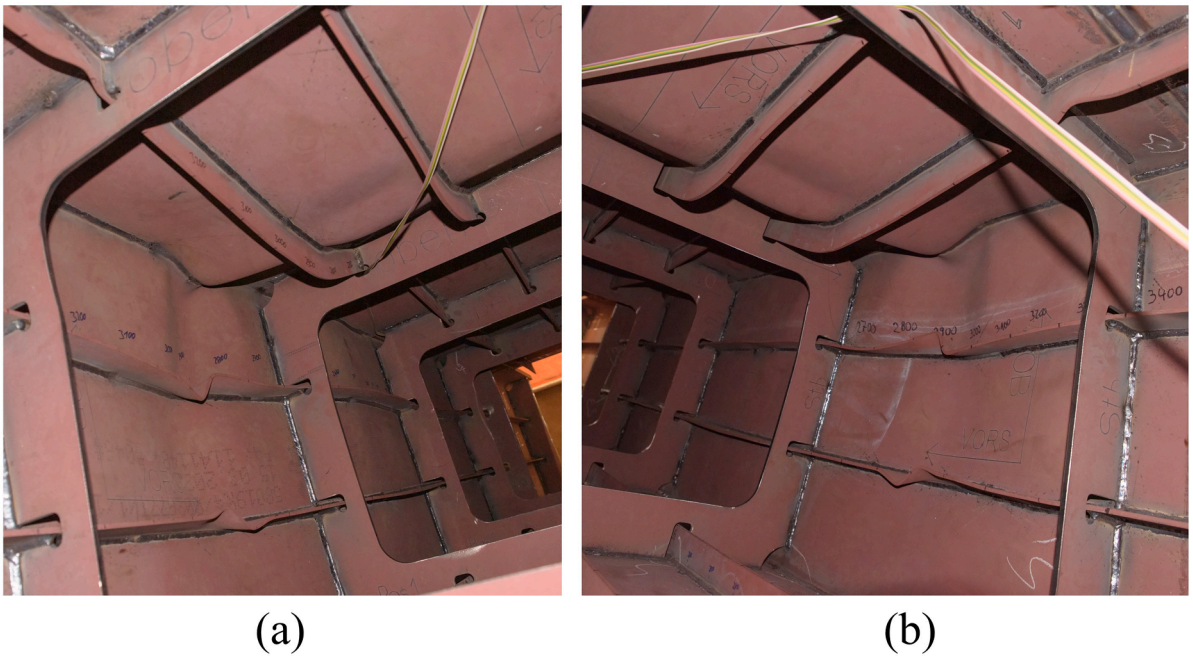

Fig. 16. Deformation of the stiffener and hull after the 1st half-cycle near division 2875 from starboard (a) and portside (b).

severe after each half-cycle, see Figs. 22 and 23. Considering the thickness of the frame, it can be inferred that the force applied on the frame is very high.

During the three half-cycles, the top and bottom in S3 always deform concavely, while the portside and starboard in S3 always deform convexly. In contrast, the overall deformation of hull plate in S2 is always opposite from that in S3. This is partly due to the deformation of longitudinal stiffeners, which represent the interaction between S2 and S3.

Fig. 17. Deformation of the stiffeners on top hull in S2, (a) - (c) refer to the results after 1st, 2nd and 3rd half-cycle respectively. In the picture, the right side is closer to starboard.

Resulting data

The data collected from the hydraulic cylinders are shown in Fig. 28, Figs. 29 and 30. The hydraulic cylinders are called as "HC" here. Referring to the positions of the hydraulic cylinders shown in Fig. 9, the force and displacement of the hydraulic cylinders at forward of the specimen are very similar, which is the same for aft. Therefore, the results are organized into groups for forward and aft. The group for forward includes HC2 and HC4, while the group for aft include HC5 and HC6. The force of each group is the total force induced by the hydraulic cylinders, and the displacement of each group is the average displacement of the hydraulic cylinders. It can be seen from the test results that, the maximum force at the hydraulic cylinders becomes lower after each half-cycle.

Since the force and displacement directly applied on the specimen are different from that measured at the hydraulic cylinders, calibration is needed. Due to the high strength of test rig (see Fig. 6), during the calibration process, the test rig is regarded as rigid for force analysis, and pure elastic for displacement analysis.

The force analysis is based on the mechanical equilibrium of the combination of cross beam and load introducer, see Fig. 31. The displacement calibration includes the deformation of test rig and the geometry relationship within it. The deformation of test rig is done by FEM analysis, see Fig. 32, where all components are modelled with elastic material and shell elements. As a result, the calibration of force and displacement are as follows:

$$F_{lf} = \frac{6462F_{cf} - 3542F_{ca}}{2920} \tag{1}$$

$$F_{la} = \frac{6462F_{ca} - 3542F_{cf}}{2920} \tag{2}$$

$$d_{lf} = \frac{F_{lf}}{456.098} + \frac{F_{la}}{644.828} + 0.197F_{lf} * 10^{-3} \tag{3}$$

$$d_{la} = \frac{F_{la}}{456.098} + \frac{F_{lf}}{644.828} + 0.197F_{la} * 10^{-3} \tag{4}$$

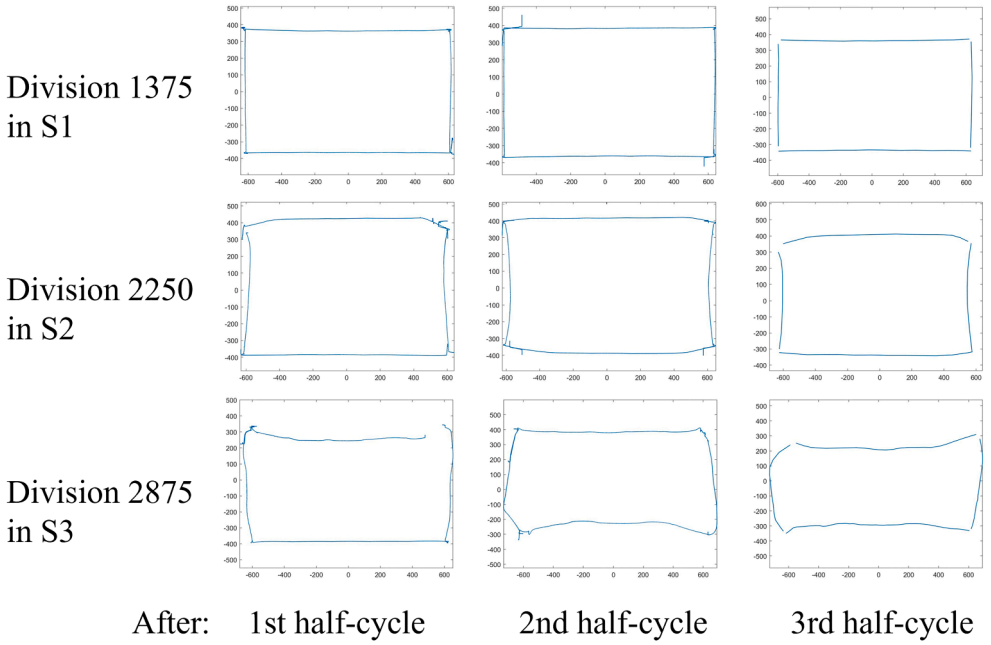

Fig. 18. Laser scan result for the outer surface of the specimen at division 1375 in S1, 2250 in S2, and 2875 in S3 after each half-cycle. Due to the limit of range from laser scanners, the surface is not always fully scanned. In all the plots, the upper side refers to the top of specimen, while left side refers to the starboard of the specimen.

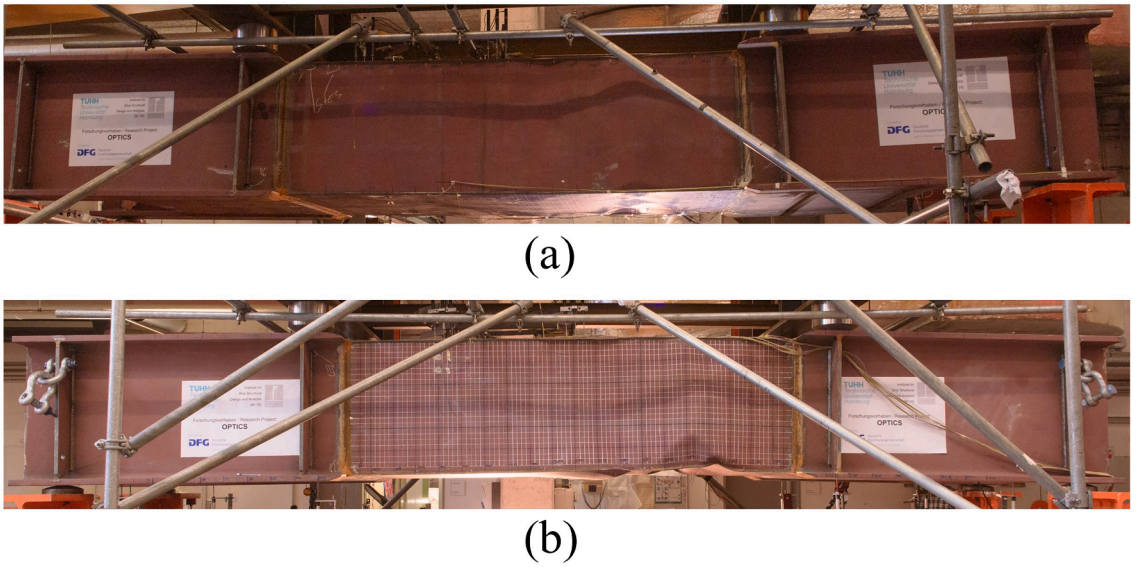

Fig. 19. During the second half-cycle (a) and third half-cycle (b), the bent specimen once "recovered" back to a "straight" box girder. However, the damage by buckling did not recover.

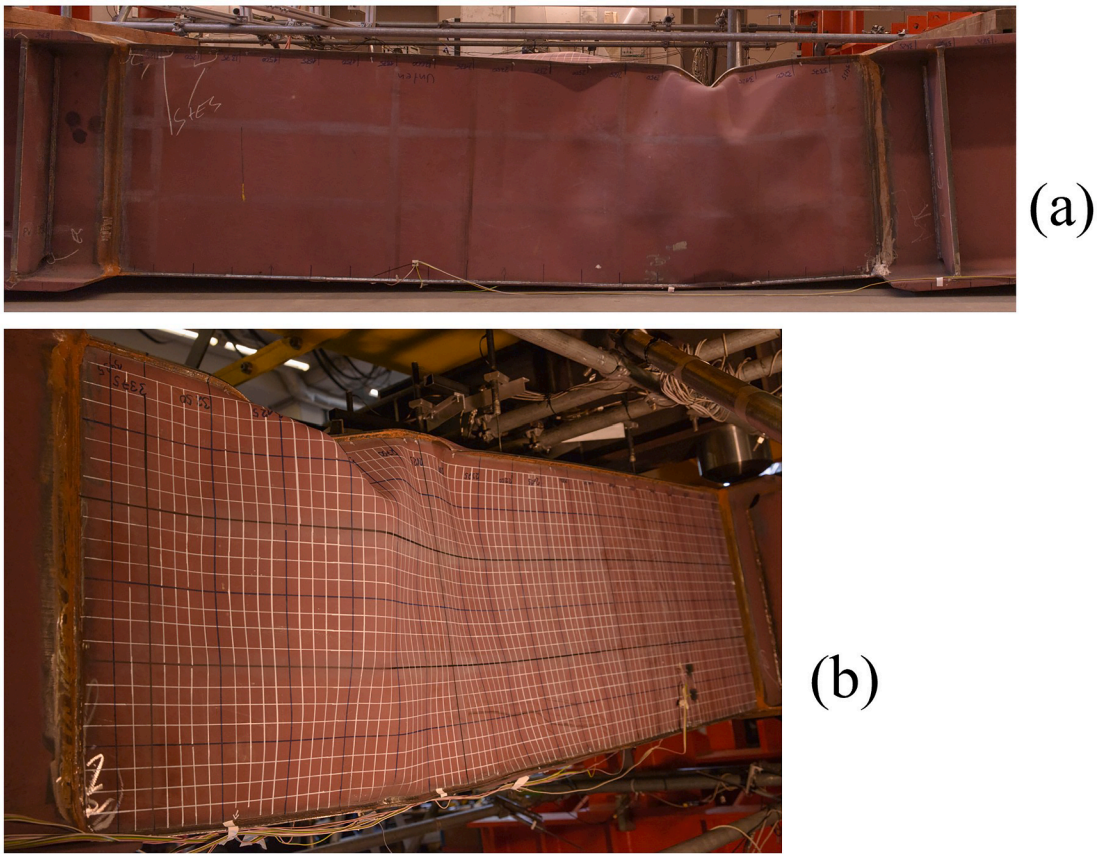

Fig. 20. Deformation of the specimen after the second half-cycle. (a) is from the view of portside, and (b) is from starboard. Since the specimen was turned for loading, the upper side of the specimen in the picture is its bottom.

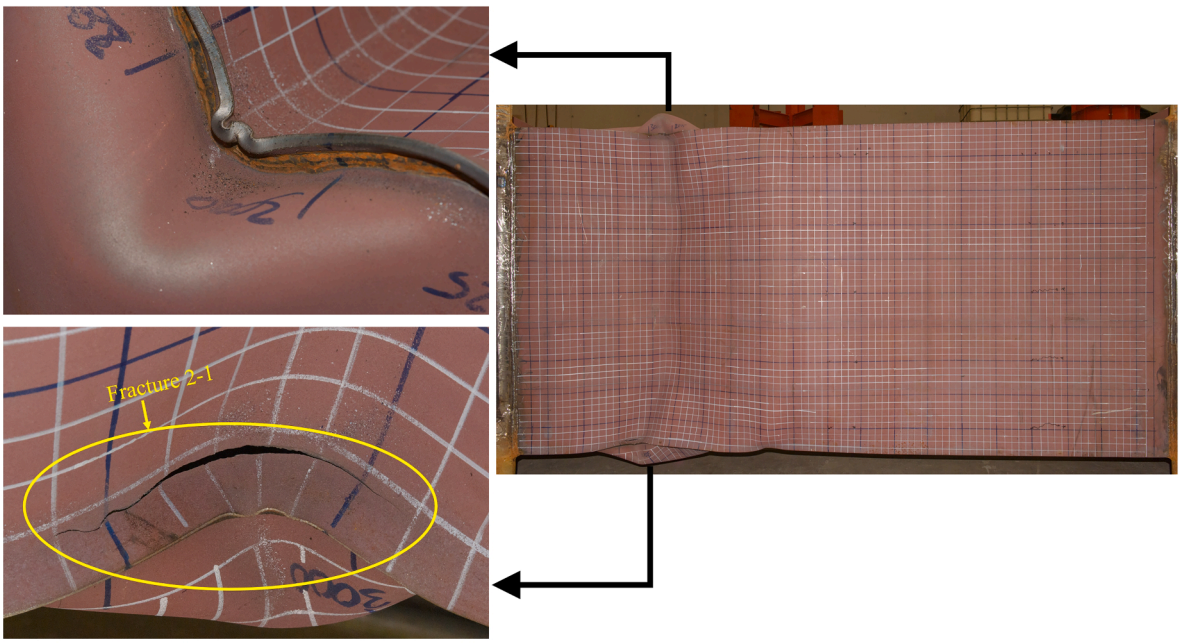

Fig. 21. Deformation of the specimen after second half-cycle, from the view of its bottom. Left side of the pictures refers to the forward of the specimen. Details in division 3000 are also shown here. The fracture 2–1 is also shown in Fig. 22.

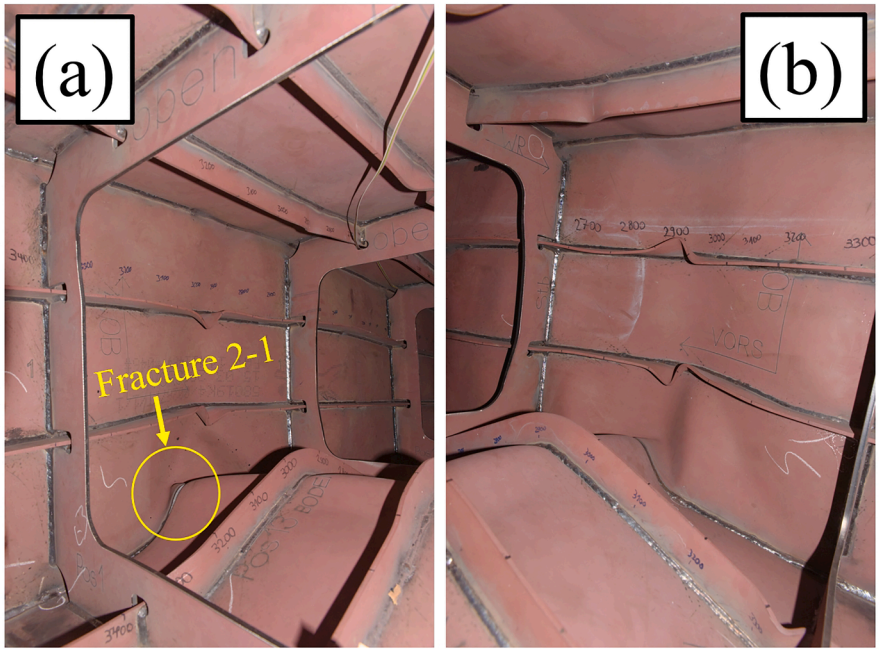

Fig. 22. Deformation of the stiffener and hull after the second half-cycle between division 2700 and 3300 on starboard (a) and portside (b). The pictures are taken from forward of the specimen. The fracture 2–1 is also shown in Fig. 21.

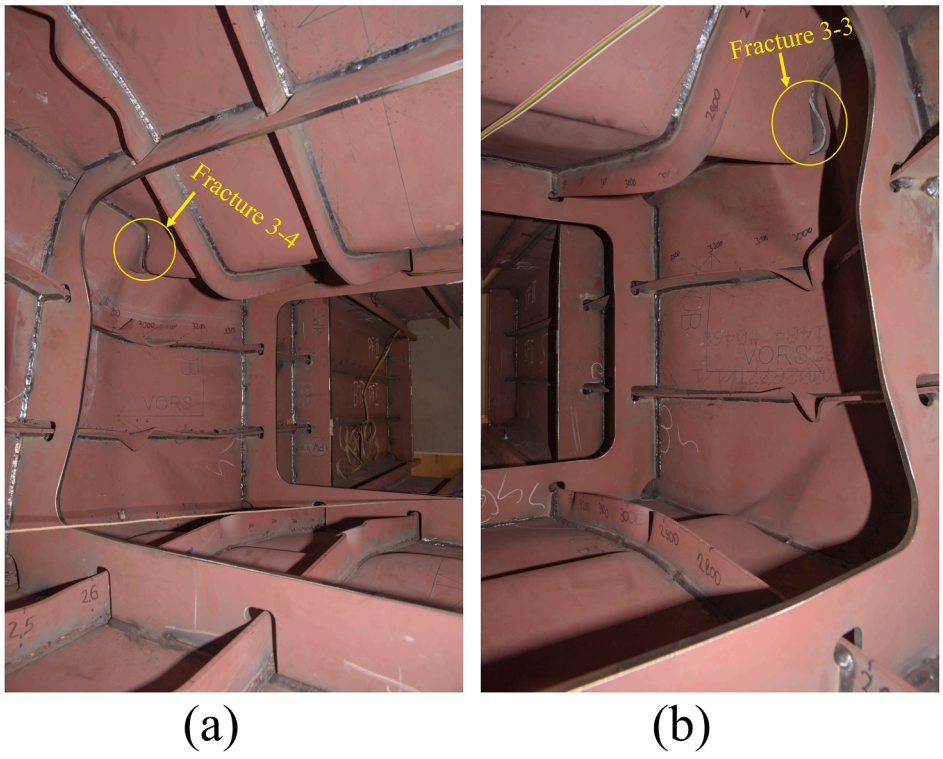

Fig. 23. Deformation of the stiffener and hull after the third half-cycle between division 2700 and 3300 on portside (a) and starboard (b). The pictures are taken from aft of the specimen. The fractures are also shown in Fig. 24, Figs. 25 and 26.

(a)

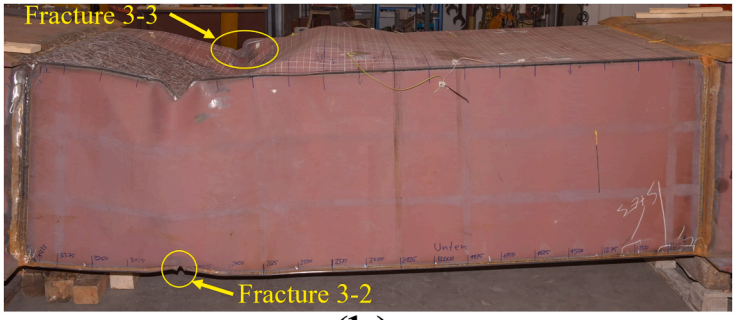

(b)

Fig. 24. Deformation of the specimen after the third half-cycle. (a) is from the view of starboard, while (b) is from portside. The fractures are also shown in Fig. 23, Fig. 25, and Fig. 26.

$$D_{lf} = \frac{6962D_{cf} - 3042D_{ca}}{10004} - d_{lf} \tag{5}$$

$$D_{la} = \frac{6962D_{ca} - 3042D_{cf}}{10004} - d_{la} \tag{6}$$

where d_{lf} and d_{la} refer to the deflection of test rig at the head of indenter on load introducer, at forward and aft side respectively, while D_{lf} and D_{la} refer to the corresponding displacements. D_{cf} and D_{ca} refer to the displacement of hydraulic cylinders at forward and aft side respectively. The nomenclature for force is the same as that shown in Fig. 31. The units are *kN* for force and *mm* for displacement. Based on the calibration above, F_{lf}, F_{la}, F_{cf} and F_{ca} for the whole test are shown in Fig. 33, where the positive direction of force is towards negative direction of the z-axis on specimen (see Fig. 4).

As is shown in Fig. 33, during the second and third half-cycles, the load applied by load introducer can be as low as zero. This is due to the unsymmetric deformation of the specimen, which leads to different deformation speed at their contact with each load introducer. As a result, the contact force between the specimen and load introducer is not always the same on each contact point.

Similar as above, the force at the supports can also be calculated as follows:

$$F_{sf} = \frac{4220F_{lf} + 1300F_{la}}{5520} \tag{7}$$

$$F_{sa} = \frac{4220F_{la} + 1300F_{lf}}{5520} \tag{8}$$

where F_{sf} and F_{sa} refer to force at support at forward and aft side of the specimen.

Based on the calculations above, referring to the divisions of the specimen shown in Fig. 4, the bending moment at division 1000 and division 3500, which are the two ends of the midsection, can be approximately calculated as follows:

$$M_{1000} = 0.21F_{la} - 1.51F_{sa} \tag{9}$$

$$M_{3500} = 0.21F_{lf} - 1.51F_{sf} \tag{10}$$

where M_{1000} and M_{3500} refer to the bending moment at division 1000 and 3500. The unit for the bending moment is $kN \cdot m$. As a result, the bending moment vs. displacement is shown in Fig. 34. Here the displacement refers to that at indenters on forward and aft side accordingly. The positive direction for bending moment corresponds with sagging of the specimen, based on the coordinate system shown in Fig. 4.

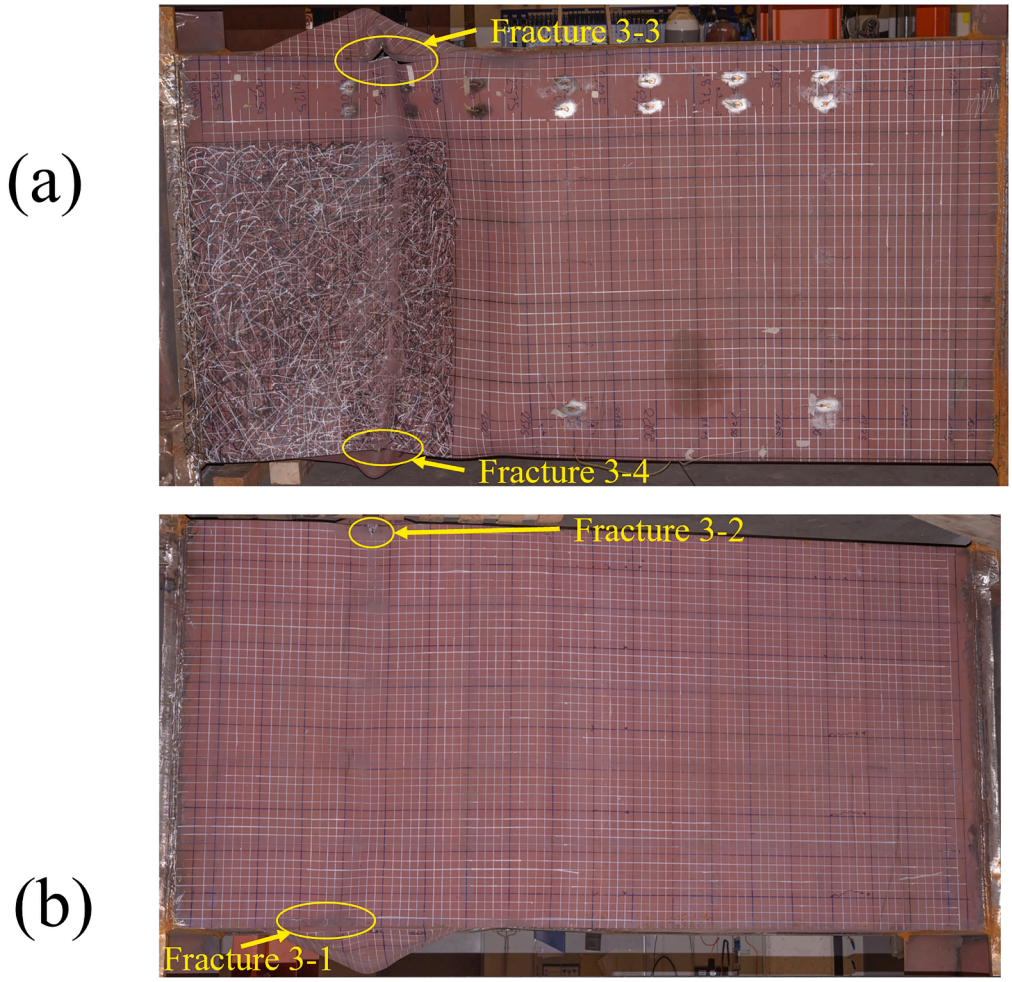

Fig. 25. Deformation of the specimen after the third half-cycle. (a) is from the view of the top. (b) is from the view of the bottom. The left side refers to the forward of the specimen. The fractures are also shown in Fig. 23, Fig. 24, and Fig. 26.

Discussions

For ultra-low cycle fatigue (ULCF) of large steel structures under alternate loading, not many research works can be found. Existing research works showed inspiring knowledge about deformation and damage of steel structures under cyclic loads, with moderate extent of damage, like plastic deformation, occurred during the test [25–27]. However, apart from the damage described in these publications, more extensive damage, such as large plastic deformation and obvious fracture can also happen during the operation of ships [7,8]. Hence, it is beneficial to investigate ULCF of ship structures under severe damage, which has not been seen in existing research works. In this study, an alternately-cyclically loaded four-point bending test is applied to a large box girder to investigate the ULCF of large steel structure. Different from pulsating loading, damage occurred in this test is induced by alternate cyclic loading. In every half-cycle, the load was intended to continue after reaching the UHGS of the specimen, which are represented by the history of force or bending moment. This test can represent the large-extent cyclic deformation and damage between sagging and hogging of a ship. During the test, the specimen does not collapse totally in only one loading process. Instead, during the cyclic loading, the damage accumulates in the specimen, causing an increasing extent of fracture and a progressive reduction of UHGS. This shows the gradual degradation of structural strength induced by plastic deformation and fracture. Such mechanical response to alternate cyclic loading is relevant to the mechanical descriptions of metal fatigue from an engineering viewpoint [31]. As a result, this test can present the ULCF of large complex structures or ship hull structures. Considering the number of cycles in the test, this study can bridge the gap between monotonic overload and ultra-low cycle fatigue.

Considering the bending moment from two ends of the midsection plotted in Fig. 34, the UHGS of the specimen is reduced after each half-cycle. Considering the large deformations showed in subsection 3.1, such reduction can be caused by multiple factors. In each half-cycle, large deformations including buckling occur in the specimen, which cause plastic deformation locally. These deformations bring additional imperfections for the following half-cycles. Moreover, the existing plastic strain reduces local material strength and leads to fracture, due to the Bauschinger effect. Moreover, taking division 2875 as an example, after each half-cycle, due to buckling

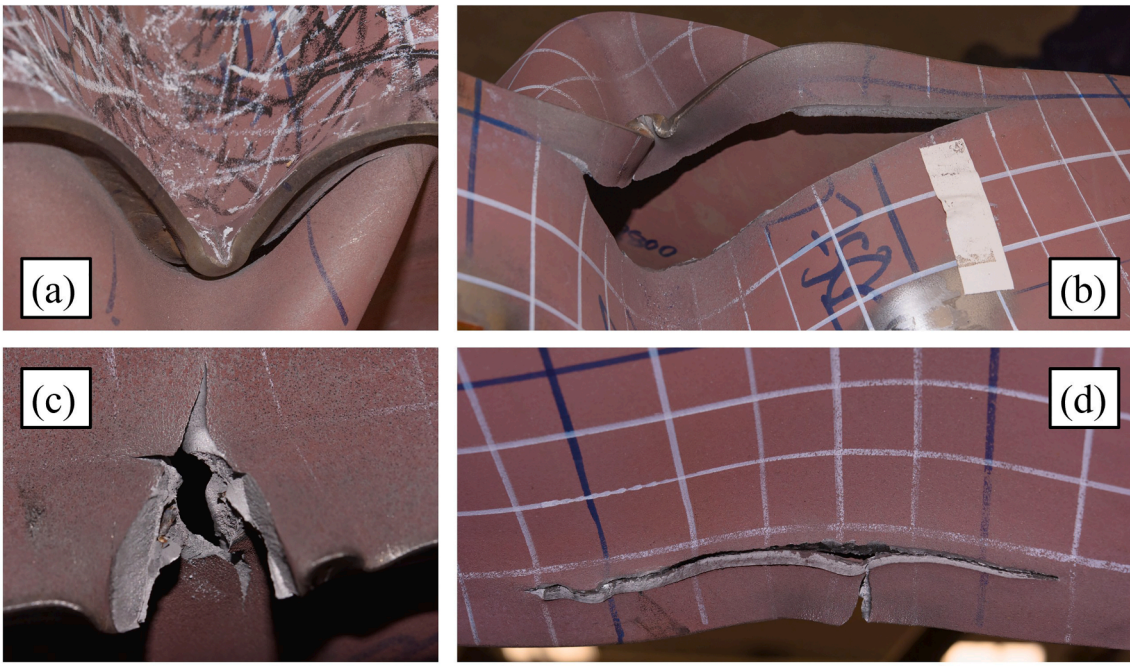

Fig. 26. Referring to the fractures after the third half-cycle shown in Fig. 23, Fig. 24, and Fig. 25: (a) fracture 3–4, between division 2875 and 3000 on top of portside, (b) fracture 3–3, between division 2625 and 3000 on top of starboard (c) fracture 3–2, between division 2875 and 3000 on bottom of portside, (d) fracture 3–1, between division 2875 and 3250 on bottom of starboard. The fracture 3–1 is grown from fracture 2–1 shown in Figs. 21 and 22.

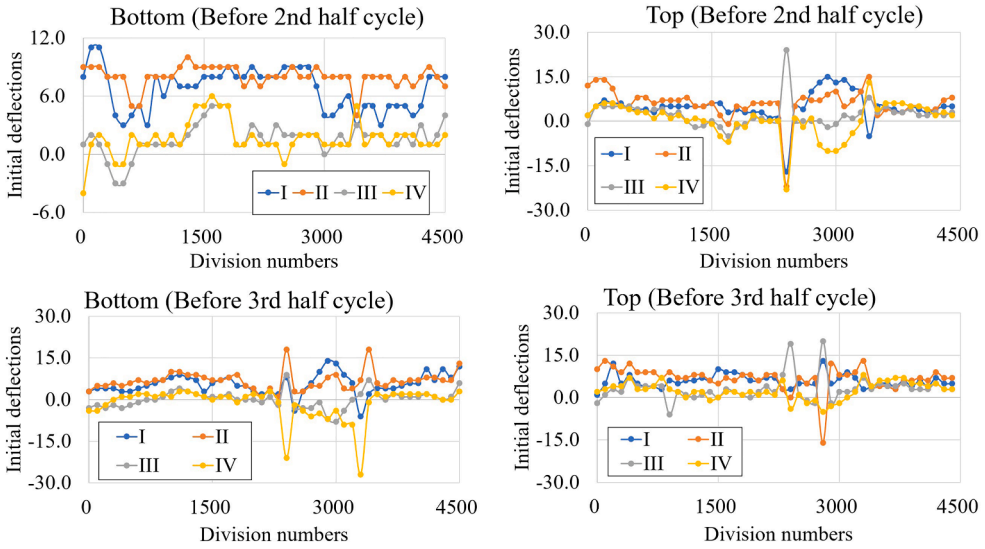

Fig. 27. Initial deflection of stiffeners on top and bottom of the specimen before second and third half-cycle.

and plastic deformation, the overall height of the section is reduced. Consequently, the components are closer to neutral plane during the bending. This will potentially reduce the moment of inertia of the section and thus its resistance against bending is reduced. As a result, during the ULCF of a structure, the UHGS is gradually reduced after each half-cycle.

Apart from the reduction of UHGS, it can be seen from the figures above that, in the second or third half-cycle, the resultant damage, e.g., deformation and fracture, is higher than those during the last half-cycle. This is also relevant to the factors mentioned above. Moreover, the loading direction also influences the accumulation of damage. In alternate cyclic loading, since the loading direction reverses after each half-cycle, the direction of deformation of the specimen also reverses. As a result, the damage in alternate cyclic loading accumulates in both hogging and sagging direction, which is different from pulsating loading. Due to the directions of

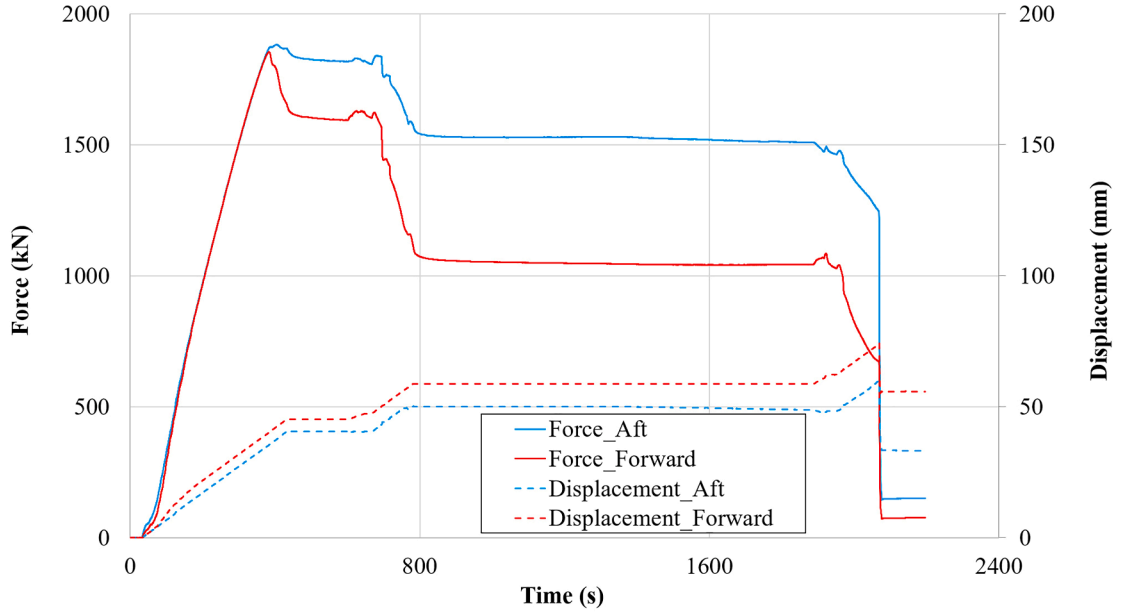

Fig. 28. Force and displacement versus time from the hydraulic cylinders, in the first half-cycle.

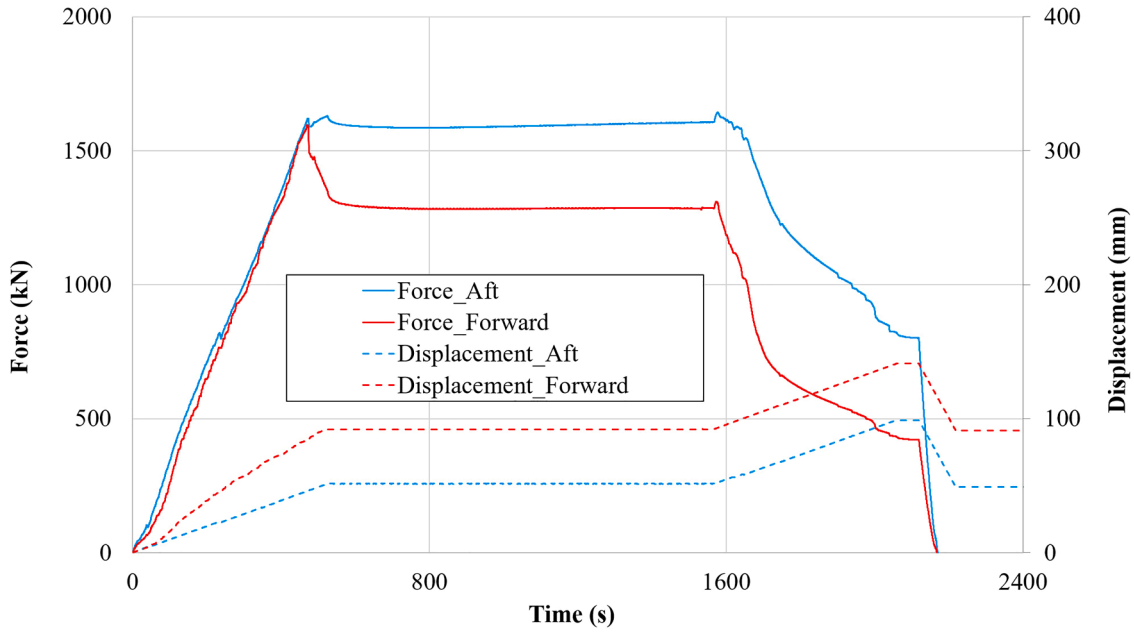

Fig. 29. Force and displacement versus time from the hydraulic cylinders, in the second half-cycle.

damage accumulation, it can be inferred that, existing damage will influence more on the loading with same direction. For example, referring to Fig. 17, the deformation of the stiffeners occurred in first half-cycle are not "recovered" during the second half-cycle. The plastic strain occurred cannot be removed as well. Therefore, the specimen is easier to deform during the third half-cycle. This also explains why the UHGS reduces significantly in the third half-cycle, compared with the reduction in the second half-cycle.

Existing large-scale bending tests often focus on the structure in one sub-section between two strong transverse/vertical stiffeners [21–23,27]. However, the interaction between adjacent sub-sections during the bending, as well as the damage of the stiffeners between sub-sections, also have great influence on the overall structural behavior. Since ship structures always include several sub-sections divided by bulkheads and stiffeners, specimens with multiple sub-sections has higher fidelity for real ship structures. In this test, comparing the resulting structural behavior in S2 and S3, although heavy damage is mostly concentrated in S3, S2 also suffered large extent of damage. Moreover, large deformation also occurred on the frame between S2 and S3, which is the strong

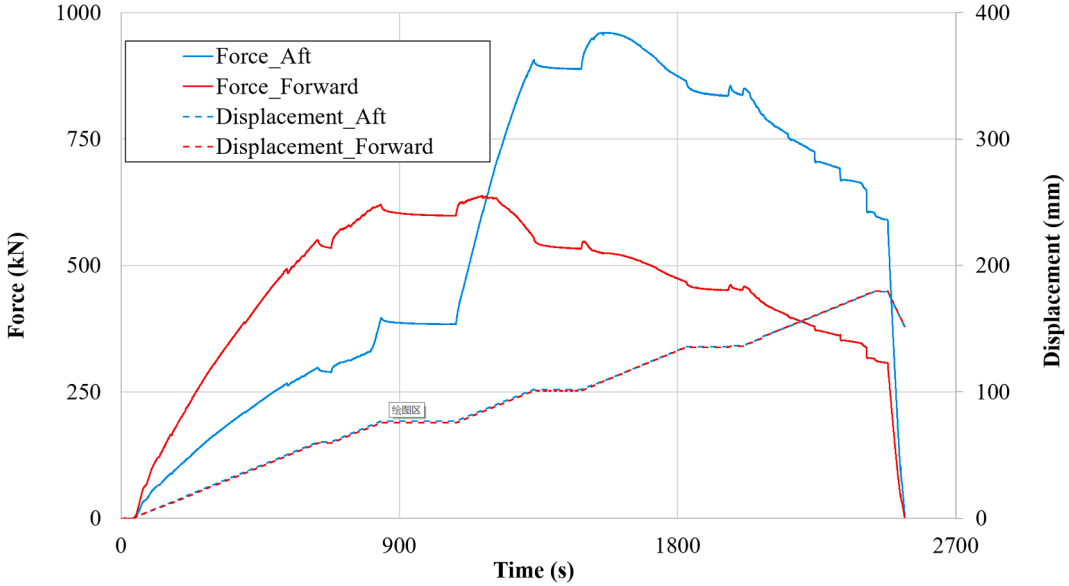

Fig. 30. Force and displacement versus time from the hydraulic cylinders, in the third half-cycle.

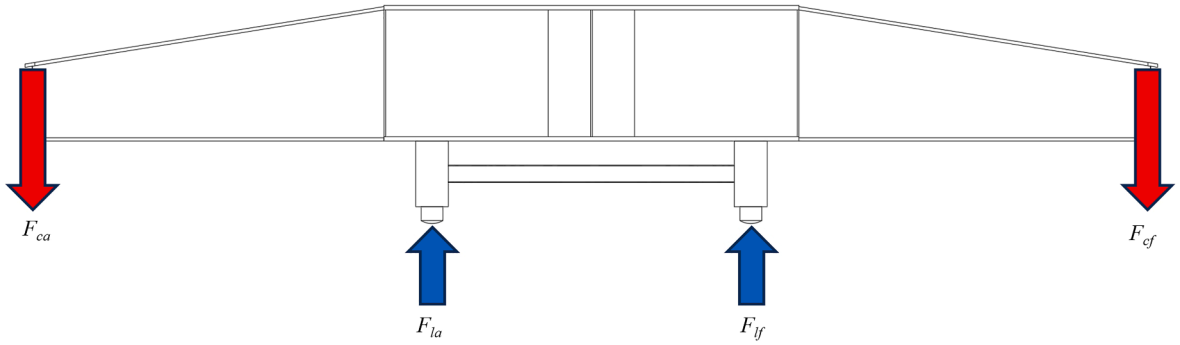

F_{cf} : Force from hydraulic cylinder (forward).
F_{lf} : Force on load introducer (forward).
F_{ca} : Force from hydraulic cylinder (aft).
F_{la} : Force on load introducer (aft).

Fig. 31. The designation of forces in the combination of cross beam and load introducer. The relevant dimensions can be found in Figs. 36 and 38.

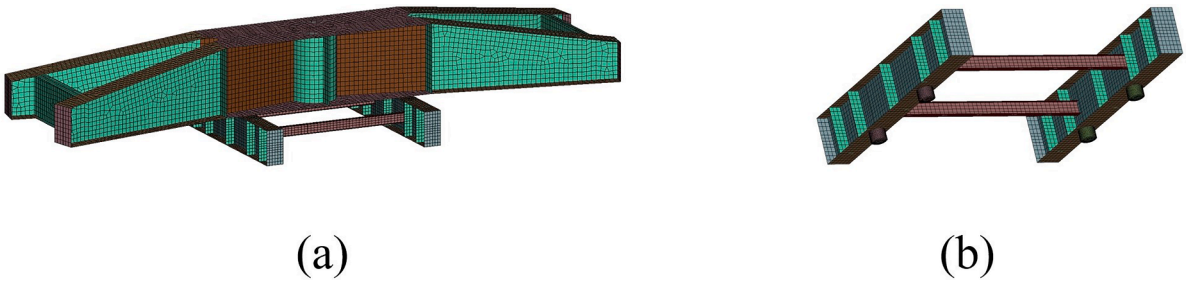

Fig. 32. FEM analysis of the cross beam (a) and the load introducer (b). The latter is shown from below.

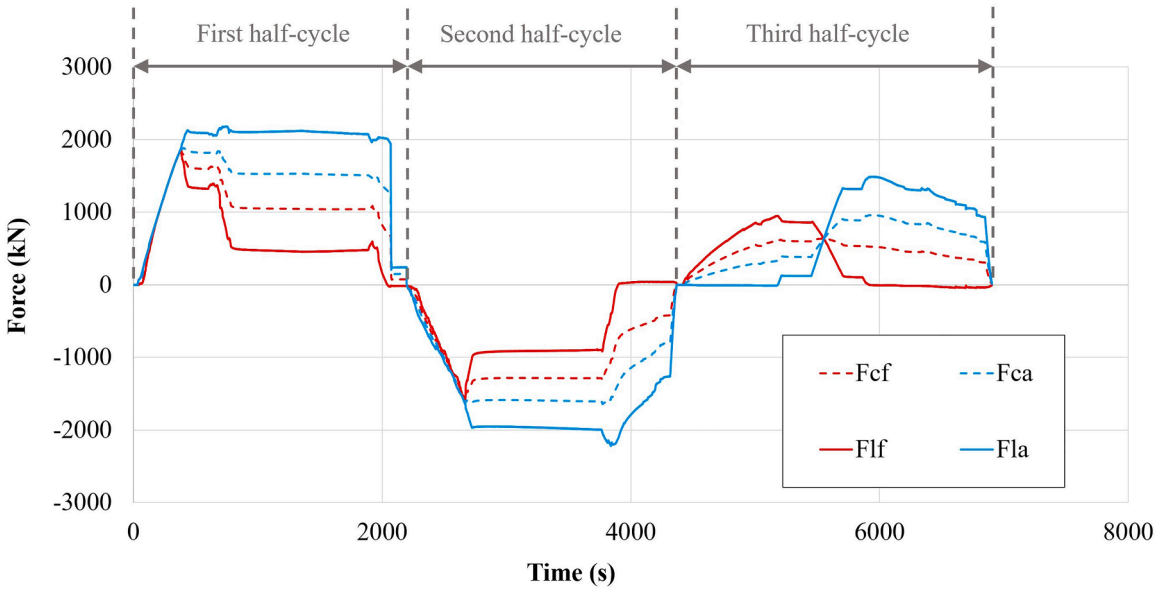

Fig. 33. The calibrated force during the whole test.

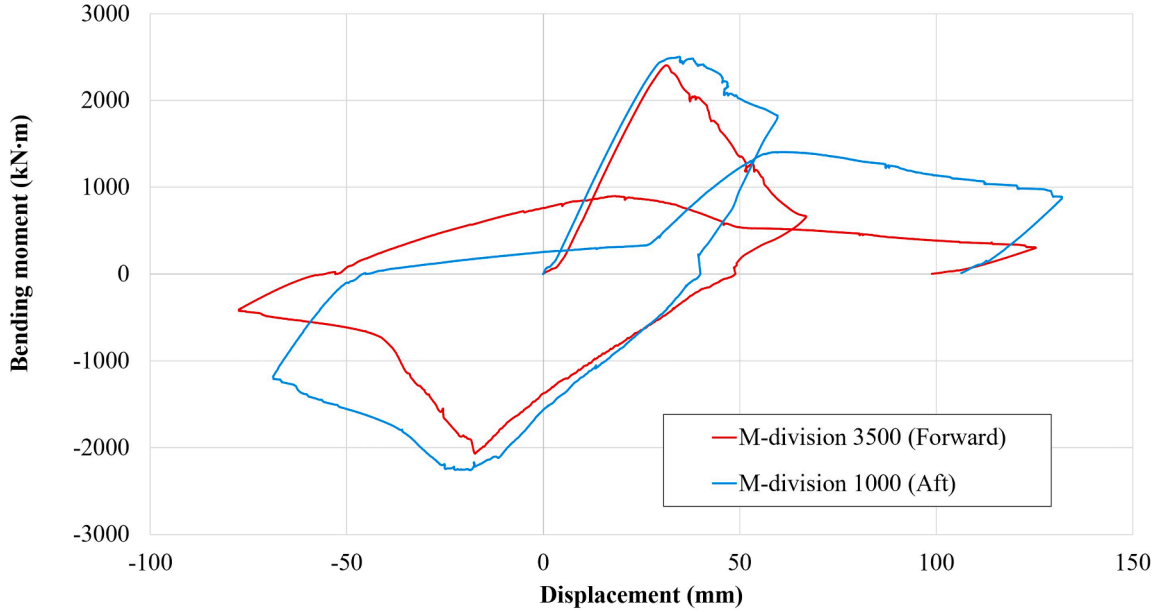

Fig. 34. Bending moment vs. displacement for the two ends of the midsection.

transverse/vertical stiffener between them. Nevertheless, compared with S2 and S3, S1 receives very few damages during the whole test. The three sub-sections of the specimen show very different structural behavior during the test. Moreover, as is mentioned above, the deformation in S2 and S3 are influencing each other. Considering the overall structural strength, although S1 was not severely damaged, the damage from S2 and S3 still introduces significant reduction of the overall hull girder strength. These results indicate that, including more sub-sections will receive more comprehensive results in large scale ULCF test for ship structures.

Conclusions

This study investigates the ultra-low cycle fatigue (ULCF) of large steel structure via experiment. In this study, a box girder with stiffeners is designed as the specimen to represent large steel structure like ships. During the test, alternately-cyclically loaded four-point bending is applied on the specimen, with three half-cycles (1.5 cycles) in total. The maximum force and bending moment are

3725.0 kN and 4842.6 kN·m respectively, thus the specimen shows strong resistance against bending. After each half-cycle, severe damages are observed in the specimen, such as buckling, plastic deformation and fracture. The existing damage also works as the initial imperfections for the next half-cycle. Based on the results of the test, conclusions are summarized as follows:

- For box girders and ship hull structures, further load after UHGS can cause severe damage to the structure, such as buckling, plastic deformation and even fracture. These damages are very possible to reduce the UHGS of the structure during cyclic loading.
- Apart from the reduction of UHGS, for the already damaged structures, once the UHGS is reached again and load continues, the follow-up damage will become more hazardous. Consequently, the structure is easier to be damaged by bending, while the extent of damage also accumulates and becomes higher, making the structure gradually weaker than before.
- Loading direction influences the damage accumulation and material behavior of the specimen in ULCF. In this study, alternate cyclic loading is applied, which can include both hogging and sagging of the specimen. Due to the opposite loading direction between each half-cycle, the damage accumulation and its influence on following loading process is different from pulsating loading. Moreover, existing damage accumulated in one loading direction will especially influence the loading and reduce the UHGS with the same direction.
- Comparing the test results in different sub-sections, the specimen shows strong asymmetry during the whole test. Moreover, despite the differences, the structural and material behavior in the three subsections still have close relations with each other. Such phenomenon is not often observable in other tests, which is due to the relatively simple structure of test sections. Therefore, for ULCF test of ship hull structures, multiple sub-sections should be included in the specimen to reveal more comprehensive results. Considering the contrasting structural behaviors of the sub-sections in this test, at least three sub-sections are recommended to be included.
- In this test, the load is introduced via four individual hydraulic cylinders, which increases the complexity and uncertainty during the test. Hence, calibration for the retrieved data is very important to correctly describe the test results.
- For ships in practice, although their structures are always designed to be strong enough for their lifetime service, accidental loads or undesired structural weaknesses still cannot be fully avoided nowadays. More investigations regarding their UHGS and post-accidental structural behavior, which are relating to ULCF of the structure, should be carried out.

The result of the test shows the structural behavior of a large complex structure suffering severe damage during alternate hogging and sagging after reaching its UHGS, which corresponds to the consequence of ULCF. The presented ULCF test also provides experiences for investigations of large complex structures with existing damages or after accidental loads. Considering the number of cycles in the test, this study can bridge the gap between monotonic overload and ultra-low cycle fatigue. Since the damage in this test consists of complex local material behavior, considering the uncertainty of the post-buckling or even post-fracture structures, it is challenging to fully clarify the material behavior in the specimen. In this case, further investigations should be made, such as high-fidelity FEM analysis of the test, or other follow-up tests.

CRediT authorship contribution statement

Shi Song: Writing – original draft, Visualization, Validation, Software, Project administration, Methodology, Investigation, Formal analysis, Data curation, Conceptualization. **Sören Ehlers:** Writing – review & editing, Validation, Supervision, Resources, Project administration, Methodology, Investigation, Funding acquisition, Conceptualization. **Franz von Bock und Polach:** Writing – review & editing, Validation, Supervision, Resources, Project administration, Methodology, Investigation, Data curation. **Moritz Braun:** Writing – review & editing, Validation, Project administration, Methodology, Investigation, Conceptualization.

Declaration of competing interest

The authors declare that they have no known competing financial interests or personal relationships that could have appeared to influence the work reported in this paper.

Funding

The presented research was funded by the Deutsche Forschungsgemeinschaft (DFG, German Research Foundation)—project number 398019838. It is stated that all funders are not responsible for any of the content of this publication.

Appendix 1. Design details of the specimen and test rig.

Table 1
The components of the specimen.

ID	Amount	Name	Dimensions (mm)	Material
1	4	Transversal frames	8.24 × 734 × 1195	Grade A36
2	1	Deck	5.66 × 1225 × 2488	Grade D36
3	1	Bottom	5.66 × 1225 × 2488	Grade D36
4	1	Side hull (portside)	5.66 × 734 × 2488	Grade D36
5	1	Side hull (starboard)	5.66 × 734 × 2488	Grade D36
6	4	Flat plate 60 × 6 – 5500 mm	6.16 × 60 × 5500	Grade A
7	8	Flat plate 60 × 6 – 4500 mm	6.16 × 60 × 4500	Grade A
8	1	HEB 800 – 1750 mm (portside, aft)	Standardized.	S235 JR
9	1	HEB 800 – 1750 mm (starboard, aft)	Standardized.	S235 JR
10	1	HEB 800 – 1750 mm (portside, forward)	Standardized.	S235 JR
11	1	HEB 800 – 1750 mm (starboard, forward)	Standardized.	S235 JR
12	1	Connection plate (aft, upper)	20 × 900.5 × 1000	Grade A36
13	1	Connection plate (aft, lower)	20 × 900.5 × 1000	Grade A36
14	1	Connection plate (forward, upper)	20 × 900.5 × 1000	Grade A36
15	1	Connection plate (forward, lower)	20 × 900.5 × 1000	Grade A36
16	8	Stiffener for HEB	20 × 141 × 734	Grade A36
17	4	Stiffener for HEB (with holes)	20 × 141 × 734	Grade A36
18	4	Stiffener for HEB (for transversal frames)	20 × 141 × 734	Grade A36

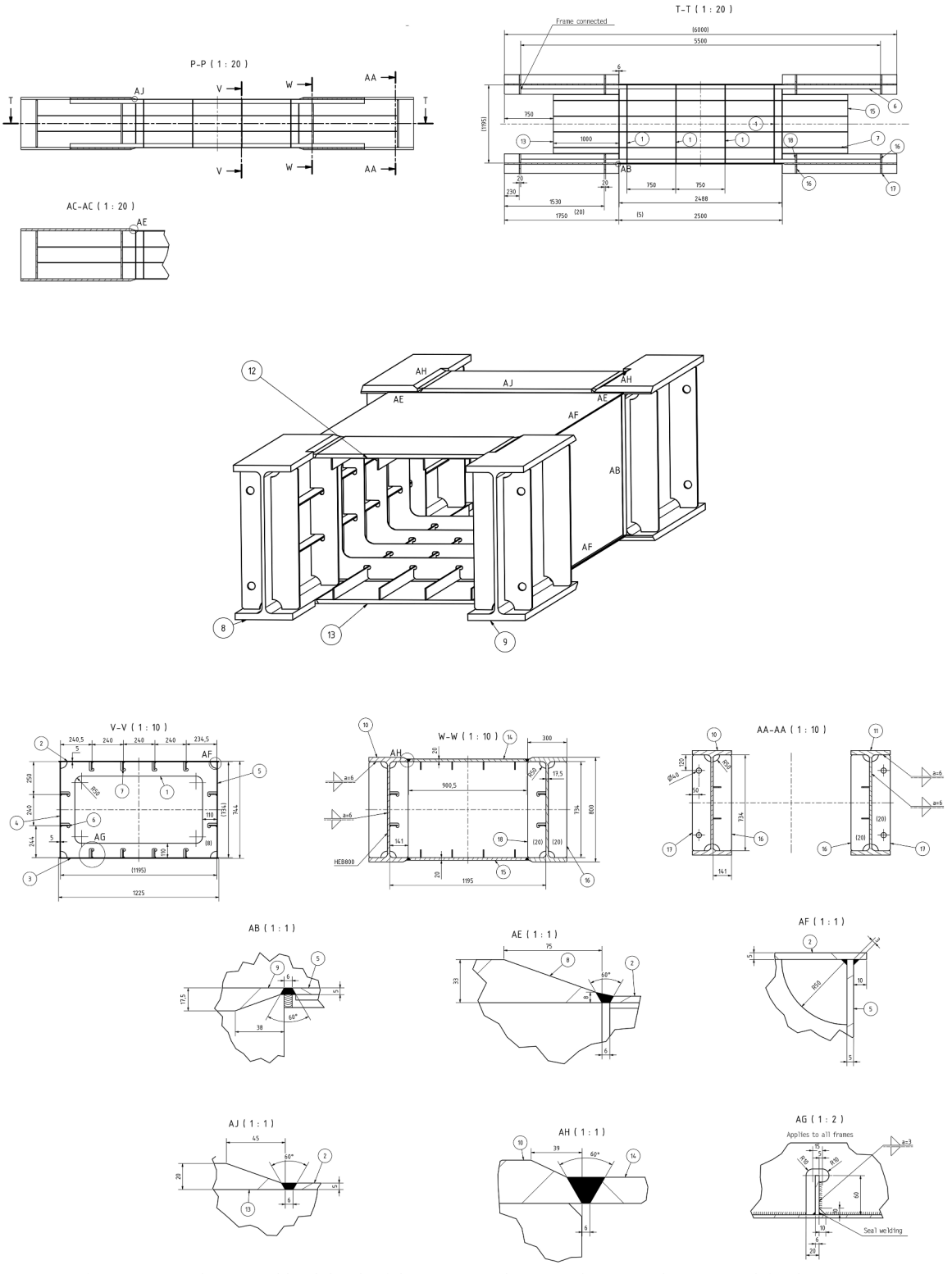

Fig. 35. Sectional views and local details of the specimen. The section line P-P and AC-AC are defined in Fig. 1.

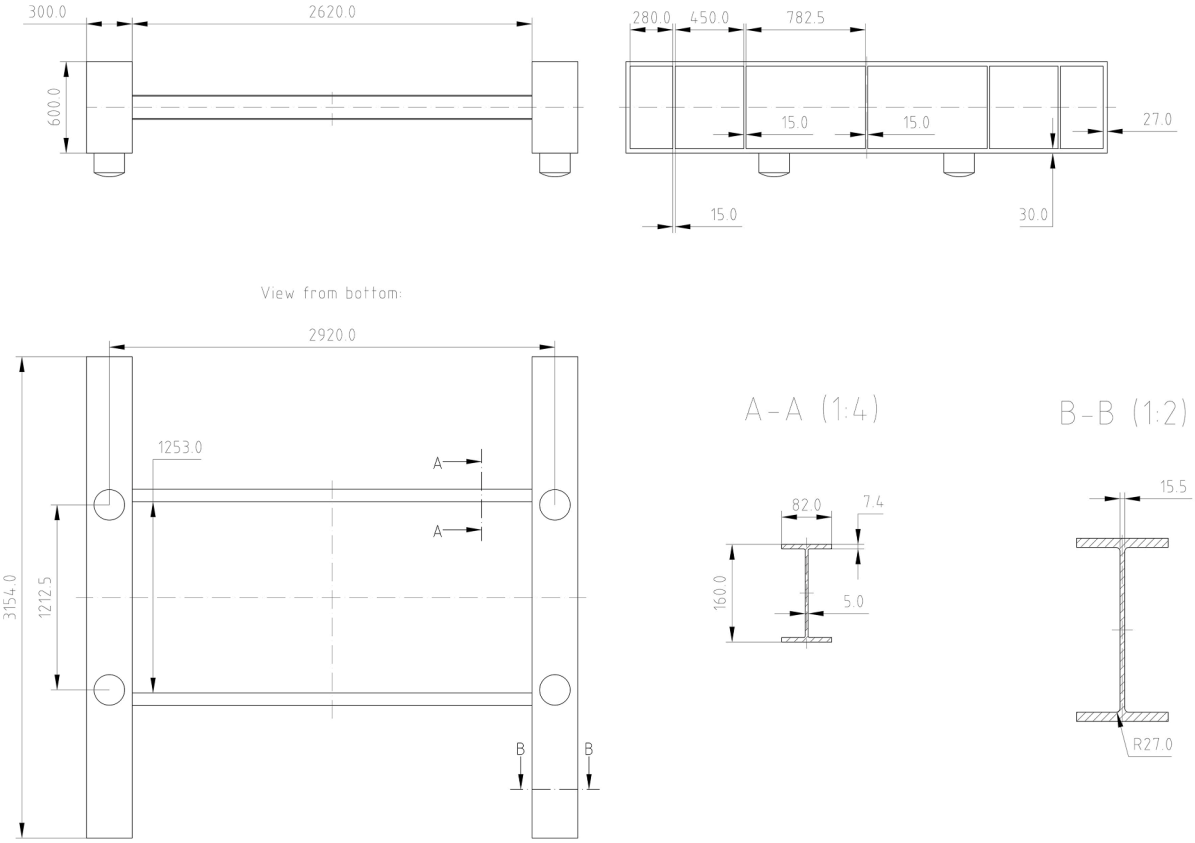

Fig. 36. Design of the load introducer.

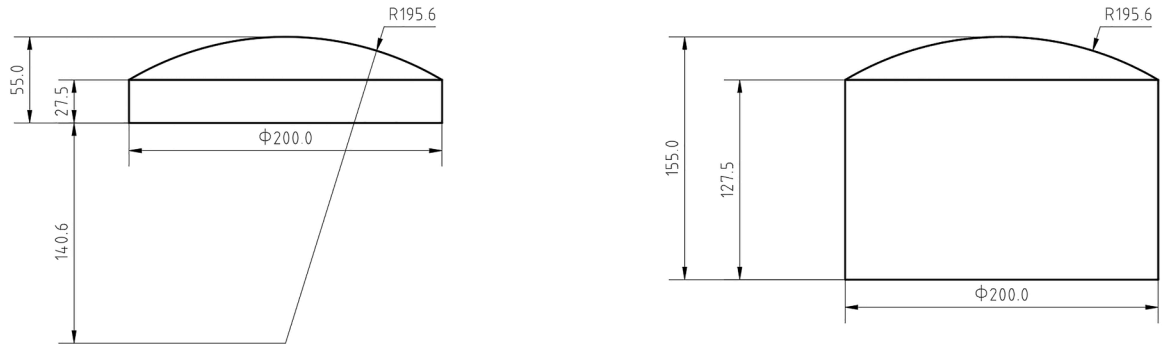

Fig. 37. The design of the support head (left) and the indenter (right).

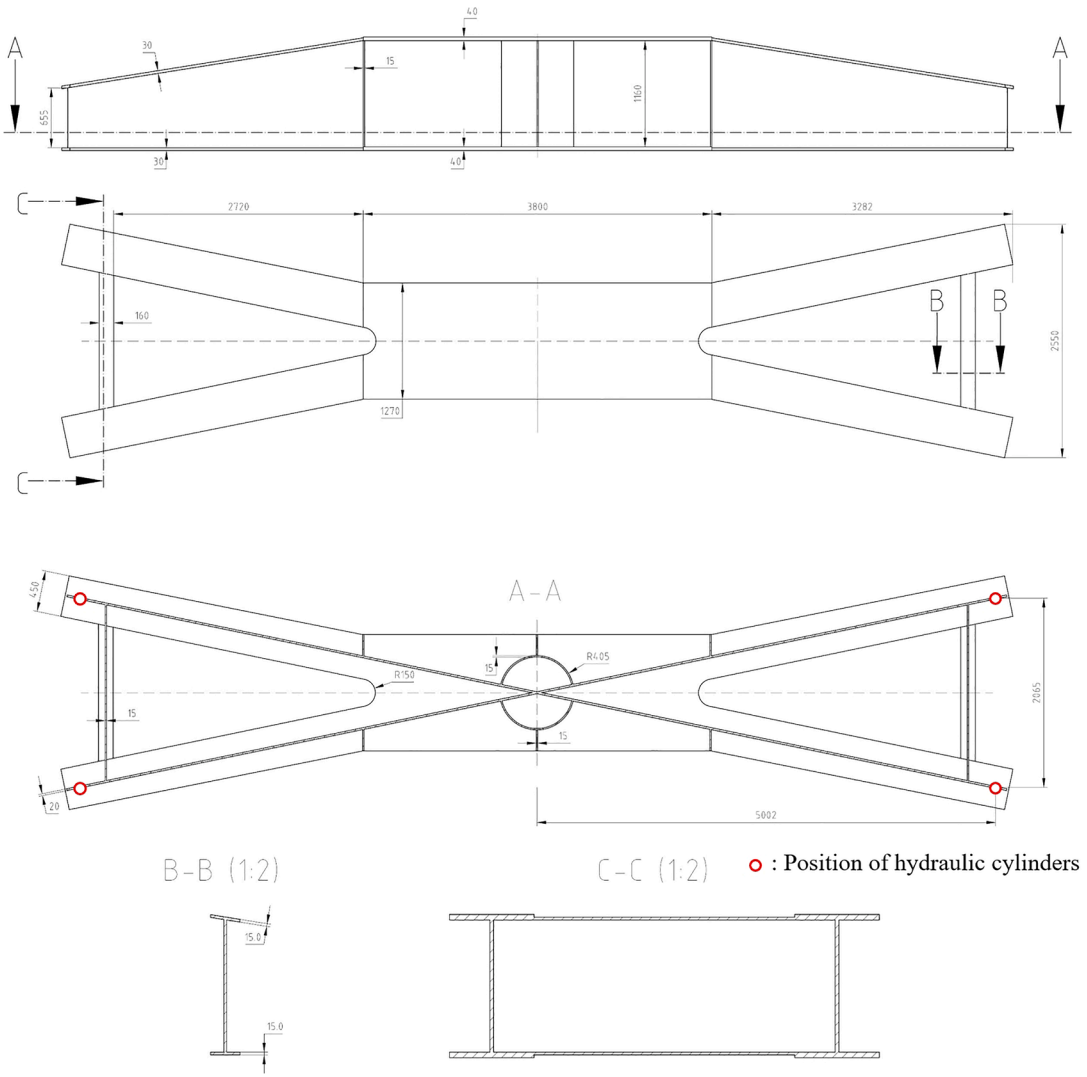

Fig. 38. The dimensions of the cross beam. The connections with the hydraulic cylinder are not shown here.

Data availability

Data will be made available on request.

References

[1] Pereira JCR, de Jesus AMP, Xavier J, Fernandes AA. Ultra low-cycle fatigue behaviour of a structural steel. Eng Struct 2014;60:214–22. https://doi.org/10.1016/j.engstruct.2013.12.039.
[2] Amiri HR, Aghakouchak AA, Shahbeyk S, Engelhardt MD. Finite element simulation of ultra low cycle fatigue cracking in steel structures. J Constr Steel Res 2013;89:175–84. https://doi.org/10.1016/j.jcsr.2013.07.007.
[3] Li S, Xie X, Tian Q, Zhang Z, Cheng C. A proposal on ultra-low cycle fatigue damage evaluation of structural steels. Theor Appl Fract Mech 2021;114:102973. https://doi.org/10.1016/j.tafmec.2021.102973.
[4] Yu M, Xie X, Cheng C. Ultra-low cycle fatigue evaluation method for unstiffened steel piers using fiber model. J Constr Steel Res 2024;213:108373. https://doi.org/10.1016/j.jcsr.2023.108373.
[5] Cheng C, Xie X, Yu M. A parametric investigation on ultra-low cycle fatigue damage of steel bridge piers under horizontal bi-directional seismic excitations. Int J Steel Struct 2024. https://doi.org/10.1007/s13296-024-00873-0.
[6] Ghaderi M, Gerami M, Vahdani R. A comparison of seismic low cycle fatigue and extremely low cycle fatigue on steel moment frames with reduced beam section connection (RBS). Int J Fatigue 2019;119:139–49. https://doi.org/10.1016/j.ijfatigue.2018.09.010.
[7] Bahamas Maritime Authority (BMA). Report of the investigation into the sinking of the "MOL comfort" in the Indian Ocean. 2015.
[8] ClassNK. Investigation report on structural safety of large container ships. 2014.
[9] Yao T. Hull girder strength. Mar Struct 2003;16:1–13. https://doi.org/10.1016/S0951-8339(02)00052-7.

[10] Sugimura T, Nozaki M, Suzuki T. Destructive experiment of ship hull model under longitudinal bending. J Zosen Kiokai 1966;1966:209–20. https://doi.org/10.2534/jjasnaoe1952.1966.209.
[11] Paik JK, Kumar YVS, Lee JM. Ultimate strength of cracked plate elements under axial compression or tension. Thin-Walled Struct 2005;43:237–72. https://doi.org/10.1016/j.tws.2004.07.010.
[12] Ringsberg JW, Darie I, Nahshon K, Shilling G, Augusto M, Benson S, et al. The ISSC 2022 committee III . 1-Ultimate strength benchmark study on the ultimate limit state analysis of a stiffened plate structure subjected to uniaxial compressive loads. Mar Struct 2022;79:103026. https://doi.org/10.1016/j.marstruc.2021.103026.
[13] Wang C, Wu J, Wang D. Experimental and numerical investigations on the ultimate longitudinal strength of an ultra large container ship. Ocean Eng 2019;192:106546. https://doi.org/10.1016/j.oceaneng.2019.106546.
[14] Czujko J., Bayatfar A., Smith M., Xu M.C., Wang D., Lützen M., et al. Committee Iii.1 ultimate strength. vol. 1. 2018. https://doi.org/10.3233/978-1-61499-862-4-335.
[15] Li S, Hu Z, Benson S. Progressive collapse analysis of ship hull girders subjected to extreme cyclic bending. Mar Struct 2020;73:102803. https://doi.org/10.1016/j.marstruc.2020.102803.
[16] Li D, Chen Z. Progressive collapse analysis and ultimate strength estimation of continuous stiffened panel under longitudinal extreme cyclic load and lateral pressure. Ocean Eng 2023;285:115340. https://doi.org/10.1016/j.oceaneng.2023.115340.
[17] Amlashi HKK, Moan T. Ultimate strength analysis of a bulk carrier hull girder under alternate hold loading condition - A case study. Part 1: nonlinear finite element modelling and ultimate hull girder capacity. Mar Struct 2008;21:327–52. https://doi.org/10.1016/j.marstruc.2007.12.006.
[18] Liu B, Guedes Soares C. Ultimate strength assessment of ship hull structures subjected to cyclic bending moments. Ocean Eng 2020;215:107685. https://doi.org/10.1016/j.oceaneng.2020.107685.
[19] Li S., Hu Z.Q., Benson S.D. A cyclic progressive collapse method to predict the bending response of a ship hull girder. Trends Anal Des Mar Struct - Proc 7th Int Conf Mar Struct MARSTRUCT 2019 2019;2019:149–57. https://doi.org/10.1201/9780429298875-16.
[20] Fricke W, Friedrich N, Musumeci L, Paetzold H. Low-cycle fatigue analysis of a web frame corner in ship structures. Weld World 2014;58:319–27. https://doi.org/10.1007/s40194-014-0117-z.
[21] Gordo JM, Soares CG. Tests on ultimate strength of hull box girders made of high tensile steel. Mar Struct 2009;22:770–90. https://doi.org/10.1016/j.marstruc.2009.07.002.
[22] Gordo JM, Guedes Soares C. Experimental evaluation of the ultimate bending moment of a box girder. Mar Syst Ocean Technol 2004;1:33–46. https://doi.org/10.1007/BF03449192.
[23] Gordo JM, Guedes Soares C. Experimental analysis of the effect of frame spacing variation on the ultimate bending moment of box girders. Mar Struct 2014;37:111–34. https://doi.org/10.1016/j.marstruc.2014.03.003.
[24] Deng H, Yuan T, Gan J, Liu B, Wu W. Experimental and numerical investigations on the collapse behaviour of box type hull girder subjected to cyclic ultimate bending moment. Thin-Walled Struct 2022;175:109204. https://doi.org/10.1016/j.tws.2022.109204.
[25] Fukumoto Y, Kusama H. Cyclic Bending Tests of Thin-Walled Box Beams. Doboku Gakkai Rombun-Hokokushu/Proceed Japan Soc Civ Eng 1985;2:141–51. https://doi.org/10.2208/jscej.1985.356_141.
[26] Akhras G, Gibson S, Yang S, Morchat R. Ultimate strength of a box girder simulating the hull of a ship. Can J Civ Eng 1998;25:829–43. https://doi.org/10.1139/l98-017.
[27] wei Cui H, P Yang. Ultimate strength and failure characteristics research on steel box girders under cyclic-bending moments. J Mar Sci Technol 2018;23:926–36. https://doi.org/10.1007/s00773-017-0521-3.
[28] Fricke W., Schöttelndreyer M., Tautz I. Validierung von Kollisionsberechnungen durch Großversuche an Konstruktionsvarianten von Seitenhüllen - Abschlussbericht BMWI- Vorhaben ELKOS 03SX284B. 2014. https://doi.org/10.2314/GBV:819246204.
[29] Lehmann E., Martens I., Fricke W. Sollbruchstellen in der Doppelhülle von Seeschiffen, Teilprojekt: durchführung von Kollisionsuntersuchungen zur Validierung von FEM-Berechnungen : abschlussbericht ; Laufzeit: 01.06.2008 - 30.04.2009. 2009. https://doi.org/10.2314/GBV:618533923.
[30] Sowerby R, Uko DK, Tomita Y. A review of certain aspects of the Bauschinger effect in metals. Mater Sci Eng 1979;41:43–58. https://doi.org/10.1016/0025-5416(79)90043-0.
[31] Pook L. Metal fatigue: what it is, why it matters, 145. Dordrecht: Springer; 2007.